2014

CHARACTERIZATION AND KINETIC ANALYSIS OF NOVEL DI-ARYL-SUBSTITUTED ISOXAZOLE HYDRAZONE ANALOGUES AT THE L-CYSTINE/L-GLUTAMATE EXCHANGER SYSTEM XC-

Jayme Lee Hartzell
The University of Montana

CHARACTERIZATION AND KINETIC ANALYSIS OF NOVEL DI-ARYL-

SUBSTITUTED ISOXAZOLE HYDRAZONE ANALOGUES AT THE L-CYSTINE/L-

GLUTAMATE EXCHANGER SYSTEM XC-

By

JAYME LEE HARTZELL

Doctor of Pharmacy, University of Montana, Missoula, MT, 2014

Thesis

presented in partial fulfillment of the requirements
for the degree of

Master of Biomedical and Pharmaceutical Sciences
in Major, Option Pharmaceutical Sciences

The University of Montana
Missoula, MT

May 2014

Approved by:

Sandy Ross, Dean of The Graduate School
Graduate School

Richard Bridges, Chair
Biomedical and Pharmaceutical Sciences Department

Sarj Patel, Co-Chair
Biomedical and Pharmaceutical Sciences Department

Philippe Diaz
Biomedical and Pharmaceutical Sciences Department

Donna Beall
Pharmacy Practice Department

Hartzell, Jayme, M.S., May 2014   Pharmaceutical Sciences

Characterization and Kinetic Analysis of Novel Di-Aryl-Substituted Isoxazole Hydrazone Analogues at the L-Cystine/L-Glutamate Exchanger System xc-

Chairperson: Richard Bridges

Co-Chairperson: Sarj Patel

The System x_c^- antiporter is plasma membrane transporter that mediates the exchange of extracellular L-cystine with intracellular L-glutamate. This exchange is significant within the context of the CNS because the import of L-cystine is required for the synthesis of the antioxidant glutathione, while the efflux of L-glutamate has the potential to contribute to either excitatory signaling or excitotoxic pathology. Changes in the activity of the transport system have been suggested to contribute to the underlying pathological mechanisms of a variety of CNS disorders, one of the most prominent of which is it highly enriched expression glial brain tumors. In an effort to produce more potent System x_c^- blocker, we have been using amino-3-carboxy-5-methylisoxazole propionic acid (ACPA) as a scaffold for inhibitor development. We previously demonstrated that the addition of lipophilic aryl groups to either the #4 or #5 position on the isoxazole ring markedly increased the inhibitory activity at System x_c^-. In the present work a novel series of analogues has been prepared in which aryl groups have been introduced at both the #4 and #5 positions. In contrast to the competitive action of the mono-substituted analogues, kinetic analyses indicate that the di-substituted isoxazoles block System XC--mediated uptake of ^{3}H-L-glutamate into SNB-19 activity by a noncompetitive mechanism. These new analogues appear to be the first noncompetitive inhibitors identified for this transport system, as well as being among the most potent blockers identified to date. These diaryl-isoxazoles should be of value in assessing the physiological roles and molecular structure of System x_c^-.

Table of Contents

List of Tables

List of Figures

Chapter 1. Introduction

1.1 Background on System x_c^-

System x_c^- (Sx_c^-) is an amino acid transporter that, under physiological conditions,

mediates the exchange of extracellular L-cystine (L-Cys$_2$) for intracellular L-glutamate

(L-Glu) across the plasma membrane (Bridges *et al.*, 2012b).

As an antiporter, Sx_c^- performs a 1:1 exchange of intracellular and extracellular amino

acids. The direction of this exchange is mediated by the concentration gradients of

substrates across the cell membrane. Early studies with Sx_c^- showed that the antiporter

acts in a sodium-independent, chloride-dependent, electroneutral manner; it transports L-

Cys$_2$ and L-Glu in an anionic form; and that both L-Cys$_2$ and L-Glu are capable of

inhibiting the transport of one another. Under normal physiologic conditions the

intracellular concentration of L-Glu well exceeds that of L-Cys$_2$ due in part to the uptake

of glutamate through excitatory amino acid transporters (EAAT), as well as the rapid

reduction of L-Cys$_2$ to L-cysteine (L-CysH) (Bridges *et al.*, 2012b).

Sx_c^- has been found to play a role in a variety of cells throughout different organ systems.

It has been characterized in cells such as fibroblasts, macrophages, hepatocytes,

endothelial cells, and the brush border membranes of renal tubules and the intestine

(Bannai, 1986; Burdo *et al.*, 2006; Hosoya *et al.*, 2002; Sasaki *et al.*, 2002; Sato *et al.*,

1999).   However, the majority of the focus has been on the localization of Sx_c^- within the

CNS, including neurons, glial cells, and within the blood-brain barrier (Burdo *et al.*,

2006).

Both sides of the Sx_c^- exchange reaction are potentially important in the function of the

CNS, as the import L-Cys$_2$ is needed for the synthesis of glutathione and oxidative

protection (Halliwell, 2006), while the exported L-Glu could contribute to neuronal

communication, as well as neuronal dysfunction (Bridges *et al.*, 2012a). Once inside the

cell, L-Cys$_2$ is rapidly reduced to L-CysH, which then serves as the rate-limiting

precursor for glutathione production (Sagara *et al.*, 1993). The efflux of L-CysH and

glutathione (through extracellular metabolism by γ-gluamyl-transpeptidase and

aminopeptidase N to form L-CysH) are then available to provide antioxidant precursors

to surrounding cells, such as mature neurons, which have little to no Sx$_c^-$ activity and are

therefore dependent on the uptake of L-CysH (Dringen *et al.*, 1999; Sagara *et al.*, 1993).

Beyond its antioxidant properties, glutathione has also been implicated in a variety of

regulatory pathways including modulating the activity of proteins possessing a critical

cysteine-residue; and interacting with receptors to influence signal transduction (Filomeni

et al., 2002; Janaky *et al.*, 1999; Seib *et al.*, 2011).

Conversely, excess Sx$_c^-$ activity can result in elevated synaptic and extrasynaptic

concentrations of L-Glu leading to excitotoxicity and cell death, which is seen in glial

brain tumors (Ye *et al.*, 1999) and inflammation induced by microglia (Shih *et al.*, 2006).

An example of how both of these processes interconnect is in brain tumor cells where

increased glutathione synthesis can result in chemoresistance and increased clearance of

xenobiotics (Huang *et al.*, 2005), while increased efflux of L-Glu leads to excitotoxicity

and cell death (Ye *et al.*, 1999).

The dual nature of Sx$_c^-$ to maintain glutathione levels and L-Glu homeostasis is both

advantageous and deleterious. The protective effects of glutathione are exerted through

glutathione-mediated elimination pathways, as well as reduction of oxidative damage to

proteins and lipids. The increased antioxidant properties provided by the production of

glutathione provide protection from many potentially toxic insults, including L-Glu itself.

The complex balance of these two processes has been implicated in a variety of CNS

diseases. A loss of Sx_c^- function has been implicated in the etiology of chronic cocaine

and nicotine addiction and relapse, as well as psychiatric disorders such as schizophrenia

(Baker *et al.*, 2003; Bridges *et al.*, 2012a; Knackstedt *et al.*, 2008; Madayag *et al.*, 2010).

1.2 Structure and Family Class

Sx_c^- is a member of the heteromeric amino acid transporter (HAT) family (Broer *et al.*,

2002; Palacin *et al.*, 2005). These transporters are heterodimers composed of an N-

glycosylated "heavy chain" (4F2hc, Solute Carrier SLC3 family) covalently linked via a

disulphide bond to a non-glycosylated "light chain" (xCT, SLC7A11). For this reason,

HATs are also referred to as glycoprotein-associated amino acid transporters. The 4F2hc

heavy subunit consists of an intracellular N terminus, a single transmembrane domain,

and a large extracellular C terminus. The 4F2hc subunit is thought to be responsible for

the trafficking of the light chain (the light subunit cannot reach the cell membrane

without interacting with the heavy subunit) and for cell surface expression. The xCT

subunit of Sx_c^- is thought to be responsible for the transport activity (Broer *et al.*, 2002;

Palacin *et al.*, 2005). Structural models of Sx_c^- indicate that xCT has 12 transmembrane

domains (TMDs), with N and C termini located inside the cell, and a re-entrant loop

between TMD 2 and 3 that appears to participate in substrate binding and

translocation(Gasol *et al.*, 2004) (See **Figure 1.1**).

Figure 1.1. A Heteromeric Amino Acid Structure
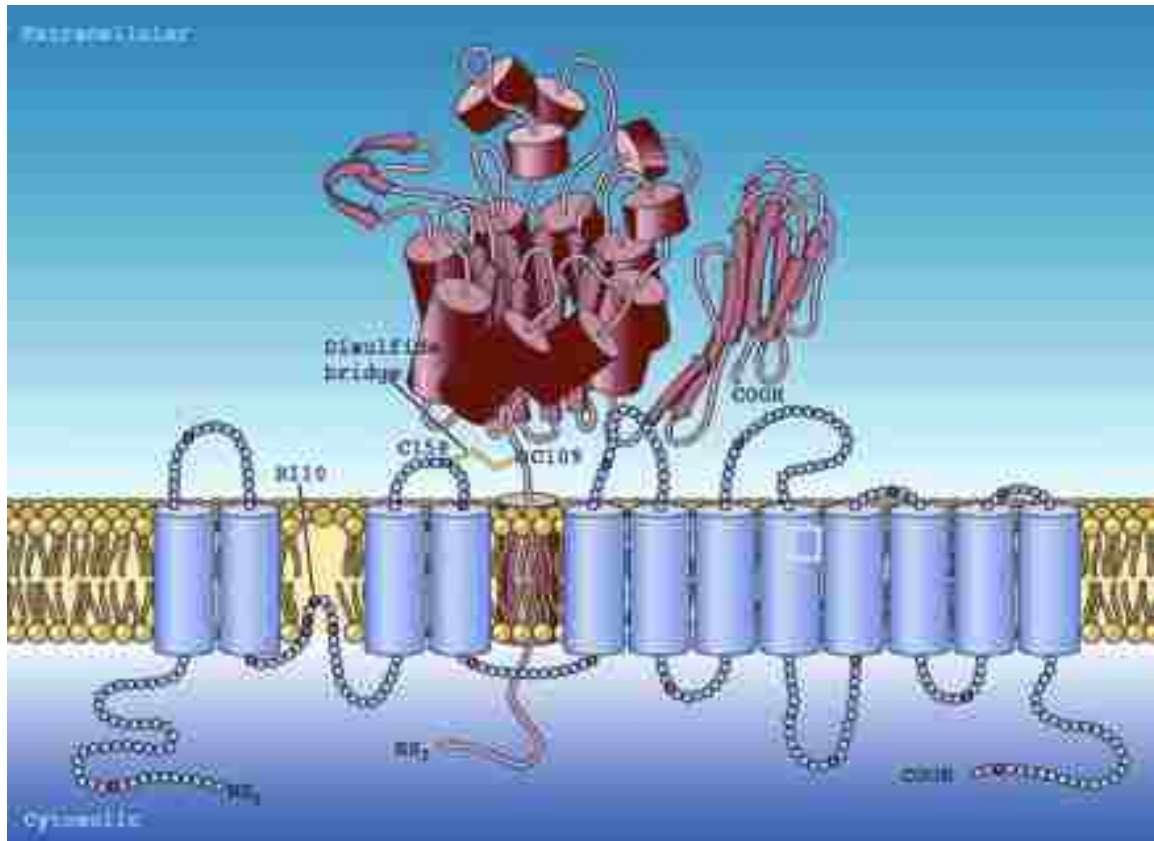
Showing the heavy-chain subunit (4F2hc) in pink, and the light-chain subunit (xCT) in blue. Palacin et al., 2005, Physiol. 20:112.

1.3 Pharmacology

Early studies with Sx_c^- focused on identifying inhibitors to provide insight into the structure activity relationships (SARs) that determine Sx_c^- selectivity, and to aid in the development of pharmacophore models.

1.3.1 Substrates/Early Inhibitors:

Initial pharmacological studies on Sx_c^- established $L-Cys_2$ and L-Glu as substrates of the transporter, as well as competitive inhibitors of each other. Structural mimics of these endogenous substrates were then used to further define key features of the transporters specificity. For example, Sx_c^- exhibits a stereo-selective preference for L-amino acids. Furthermore, use of acyclic EAA analogues with shorter, "aspartate like" chain lengths demonstrated an inability to bind at Sx_c^-, thus distinguishing it from the EAAT transport systems (Patel *et al.*, 2004). Other defining characteristics include: the ability of L-α-aminoadipate and L-α-aminopimelate to act as inhibitors (demonstrating that longer chain lengths can be tolerated); the inactivity of L-homocystine as an inhibitor (demonstrating the transporters limit to accommodate increasing chain lengths); and that SO_3^- and SO_2^- groups can replace a distal COO^- (inhibition with L-homocysteate, L-serine-O-sulphate, and L-homocysteine sulphinate), but PO_3^{2-} groups cannot (lack of inhibition with L-serine-O-phosphate) (Bridges *et al.*, 2012b).

1.3.2 Conformationally Constrained Inhibitors

In an attempt to identify more potent inhibitors for Sx_c^-, several comformationally constrained analogues of Glu where characterized (Patel *et al.*, 2004). This strategy

8

restricts bond rotation so the functional groups on the molecule can be locked in a configuration that hypothetically mimics that of the endogenous substrate when it binds the transporter. Past studies have identified four such analogues that inhibit Sx_c^-, including quisqualate (QA), 4-S-carboxy-phenylglycine (4-S-CPG), ibotenate (IBO), and (RS)-4-Br-homoibotenate. Of note, each of these compounds is also known for exhibiting activity at other iGluRs and mGluRs. Studies examining substrate activity of these analogues showed IBO to have comparable substrate activity to that of $L-Cys_2$ (Patel *et al.*, 2004). While (RS)-4-Br-homoibotenate and QA also acted as substrates, their ability to be transported was considerably less than that of IBO. The two most potent inhibitors, QA and 4-S-CPG (% of control 1±1 and 3±1, respectively) were the least active as substrates. Therefore demonstrating that the inhibitors with the highest affinities may promote binding, but preclude the translocation of the amino acid (Patel *et al.*, 2004) (refer to **Figure 2.1** in chapter 2).

The action of QA as a potent inhibitor at Sx_c^- inspired the idea for the use of isoxazoles as scaffolds for the development of additional inhibitors of the transporter (Patel *et al.*, 2010). Although QA blocked Sx_c^-, other closely related iGluR agonists, such as aminomethyl isoxazole propionic acid (AMPA) did not. Further work based on the structure of AMPA led to the development of a series of amino-3-carboxy-5-methylisoxazole propionic acid (ACPA) analogues and non-amino acid biosteres of ACPA, e.g. hydrazone acids (Matti *et al.*, 2013; Patel *et al.*, 2010). It was found that the addition of lipophilic groups to the ACPA template produced inhibitors with affinities comparable to that of $L-Cys_2$. The Sx_c^- structure activity relationship (SAR) studies allowed the distinguishing characteristics between GluR2 and Sx_c^- binding sites to be

delineated, as well as demonstrated the presence of lipophilic binding domains adjacent to the substrate-binding site within the transporter (see **Figure 1.2**). To further assess the relative position of these lipophilic domains, several 4,5-di-substituted ACPA derivatives were prepared to test whether the aryl groups were interacting with one or two distinct sites (Patel *et al.*, 2010). Although less potent than the mono-substituted isoxazoles, the use of the "hybrid" isoxazoles, which contained lipophilic substituents at both positions 4 and 5, confirmed the presence of two distinct lipophilic domains within the binding pocket. When tested for substrate activity, it was found that these 4,5-di-substituted inhibitors could not act as substrates of Sx_c^-, suggesting that even though the binding site could accommodate the added steric bulk, the additional lipophilic groups precluded translocation. In addition, extensive kinetic analysis demonstrated that the ACPA analogue, S-2-napthyl-ethyl-ACPA acted via competitive inhibition (Patel *et al.*, 2010). Along with 4-S-CPG, one of the most potent inhibitors of Sx_c^- characterized to date is sulfasalazine (SSZ; 6-oxo-3-(2-[4(N-pyridin-2ylsulphamoyl)phenyl]diazenyl-cyclohexa-1,4-dienecarboxylic acid)) (Gout *et al.*, 2001). SSZ is more commonly used for its anti-inflammatory properties in diseases such as Chron's and Rheumatoid Arthritis. As a prodrug, SSZ is broken down into sulphapyridine and 5-amino salicylic acid to exert its anti-inflammatory effect, but only the prodrug form of SSZ is capable of inhibiting activity at Sx_c^-. Although SSZ, like many Sx_c^- inhibitors, contains a benzoic acid moiety, it lacks the prototypical L-α-amino acid head group. However, SSZ maintains potency equal to that of 4-S-CPG, suggesting that portions of SSZ may interact effectively enough with other domains of the Sx_c^- binding site so that the interactions with an L-α-amino acid head group are no longer required (Bridges *et al.*, 2012b).

Figure 1.2. A Ligand-Based Pharmacophore model of Sx_c^-
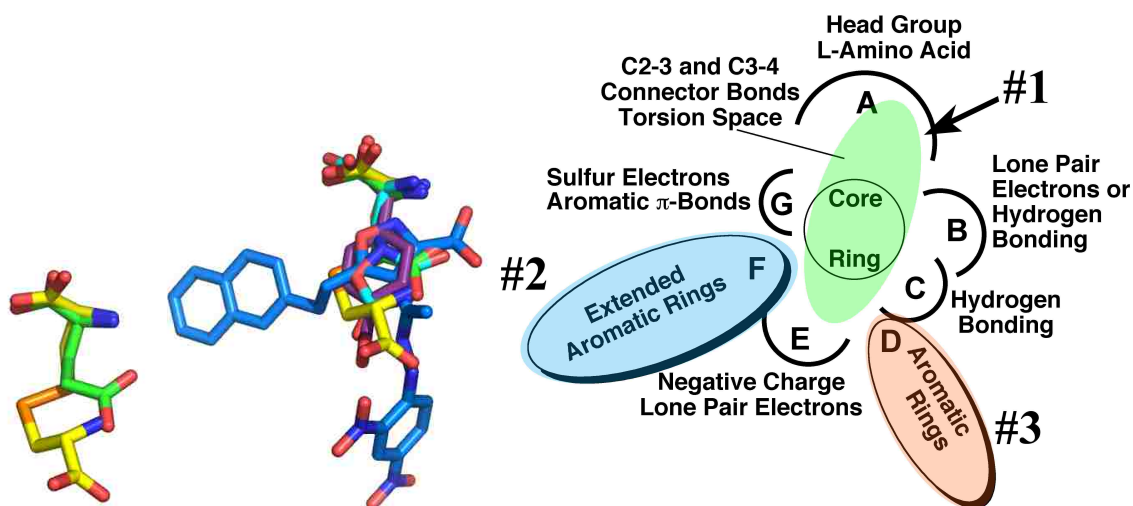
A ligand-based superposition, 3D pharmacophore model for the substrate binding on Sx_c^-.

A & B, L-Glu in green; L-Cys$_2$ in yellow; QA in teal; 4-S-CPG in purple; NACPA in red; and TFMIH in orange. F, pharmacophore binding template.

1.4 Kinetics of Transporter Inhibition

1.4.1 Competitive inhibition

One of the most common mechanisms of inhibition of transporters and enzymes is

competitive inhibition. In this mechanism, binding of the substrate and inhibitor are

mutually exclusive and only one can bind at a time. This most often occurs when the

inhibitor is binding to the same site as the substrate. In enzyme kinetics, a competitive

inhibitor acts by decreasing the number of free enzyme molecules available to bind

substrate, and eventually form product. This process is diagramed in **Figure 1.3**.

With competitive inhibition, the substrate and inhibitor exert reciprocal effects on the

concentration of EI and ES complexes.   Therefore, increasing the concentration of

substrate decreases the concentration of EI complex and raises the reaction velocity.   In

other words, by increasing the amount of substrate the inhibitor can be out-competed for

the binding site and the transporter can eventually attain its maximum velocity (or V_{max}).

The amount of substrate needed to completely overcome inhibition depends on the

concentration of inhibitor present, its affinity for the enzyme (K_i), and the K_m for the

substrate.

Figure 1.3: Enzyme Kinetics for Competitive Inhibition

$$E + S \quad \xrightleftharpoons[k_{-1}]{k_1} \quad ES \quad \xrightleftharpoons{k_2} \quad E + P$$

$$\begin{array}{c} + \\ I \end{array} \quad \updownarrow K_i$$

$$EI$$
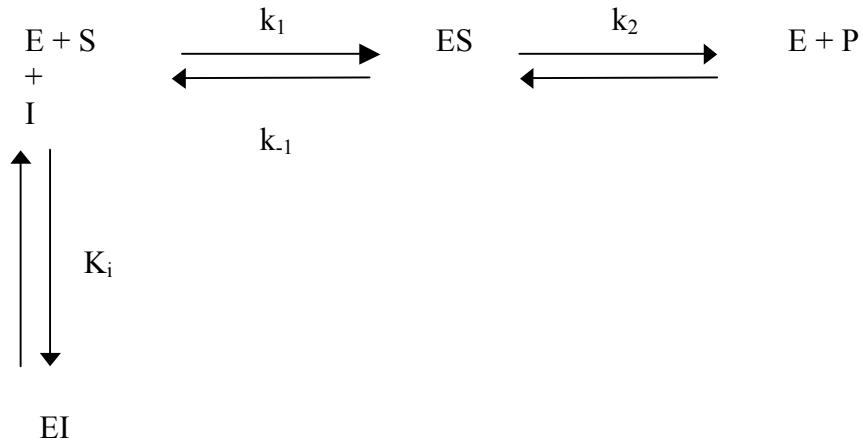
Scheme diagramming the enzyme kinetics for competitive inhibition. E, enzyme; I, inhibitor; k, rate constant; K_i, inhibitory constant; S, substrate; P, product.

For Sx_c^-, competitive inhibition is best exemplified with the endogenous substrate L-cystine. **Figure 3.1** in the supplemental data shows a graphical presentation of competitive inhibition with L-cystine using three separate kinetic analyses: a Michaelis-Menten plot, a Lineweaver-Burk plot, and an Eadie-Hofstee plot. Since increasing substrate concentration can overcome inhibition with a competitive inhibitor, the maximum transport velocity (V_{max}) remains constant. However, the apparent value of the Michaelis-Menten constant (K_m) increases. This is best seen in the Lineweaver-Burk and Eadie-Hofstee plots, where the lines intersecting at the Y-axis represent constant V_{max} values in both graphs. The K_i value for competitive inhibitors can be determined using replots of the slopes from the Lineweaver-Burk graphs vs. [I]. These replots can also be used to distinguish between competitive and noncompetitive inhibition. The replot of $K_{m.apparent}$ vs. [I] is linear for competitive mechanisms, while the replot of $V_{max.apparent}$ vs. [I] is linear for noncompetitive mechanisms (Newell *et al.*, 2013; Segel, 1993).

1.4.2 Noncompetitive inhibition

Noncompetitive inhibition occurs when the substrate and inhibitor bind reversibly and independently at different sites, meaning that the substrate can bind both E and EI, and the inhibitor can bind both E and ES complexes. This process is diagramed in **Figure 1.4**.

14

Figure 1.4: Enzyme Kinetics for Noncompetitive Inhibition

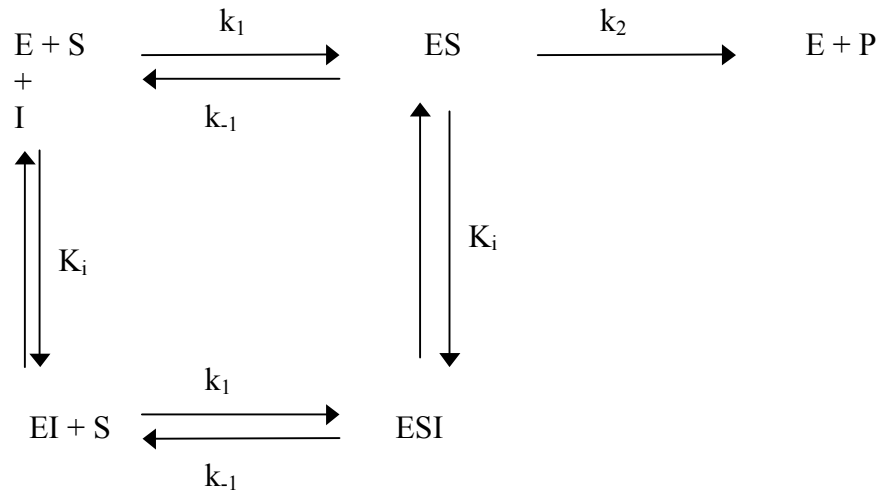$$E + S \xrightarrow[k_{-1}]{k_1} ES \xrightarrow{k_2} E + P$$

Sheme diagraming the enzyme kinetics for a noncompetitive inhibitor. E, enzyme; I, inhibitor; k, rate constant; K_i, inhibitory constant; S, substrate; P, product.

While the enzyme-inhibitor complex (or in the case of Sxc- the transporter-inhibitor complex) can still bind the substrate, its efficiency at transforming/transporting that substrate is decreased; reflected by a decrease in Vmax. However, the apparent Km value remains constant for noncompetitive inhibitors. In other words, in noncompetitive inhibition increasing the amount of substrate will not overcome the binding of the inhibitor. Therefore, the transporter will never reach its maximum velocity (Vmax) as long as there is inhibitor present. For "pure" noncompetitive inhibitors, the E and EI have equal affinity for the substrate, and the EIS complex does not generate product. In more complex types of noncompetitive inhibition, the binding of the inhibitor does affect the apparent affinity of the enzyme for the substrate, causing the lines of the double-reciprocal plot (Lineweaver-Burk plot) to intersect in the third or fourth quadrant (meaning the transporter has less affinity for the substrate, represented by a higher $Km_{apparent}$ value) (Segel, 1993).

These more complex mechanisms of noncompetitive inhibition can also be evaluated by using replots from the Lineweaver-Burk graphs of slope vs. [I] and $1/V_{max.apparent}$ vs. [I]. If both the slope and the $1/V_{max.apparent}$ replots yield similar K_i values, the analogue is considered to be acting as a "pure" noncompetitive inhibitor (where the binding of the inhibitor does not alter the binding of the substrate); see **Figure 3.8** of supplemental data. However, if the K_i value from the $1/V_{max.apparent}$ vs. [I] is considerably higher than that of the K_i value from the slope vs. [I], this would suggest that the binding of the inhibitor decreases the affinity with which the transporter binds the substrate; see **Figure 3.4** of supplemental data (Segel, 1993).

1.5 Present Work with Sx_c^-

Previous studies carried out by our lab have demonstrated that isoxazoles with lipophilic modifications at either the #4 or #5 position of the heterocyclic ACPA base structure exhibit increased inhibitory activity at Sx_c^-. In the present work, a novel set of isoxazole compounds containing lipophilic aryl groups at both the #4 and #5 positions were developed and assessed for inhibitory activity at Sx_c^-. The development of di-substituted analogues was used to confirm the presence of multiple lipophilic binding pockets within the binding site. These 4,5-di-subsituted analogues also underwent extensive kinetic analysis to characterize their mechanism of inhibition. As will be seen in the following chapter, our structure activity studies have led to the identification of both competitive and noncompetitive inhibitors. A select sample of these inhibitors will be presented in Chapter 2, and an expanded library of compounds is presented in Chapter 3. Demonstration of noncompetitive inhibition is a very interesting discovery since no noncompetitive inhibitors have been developed for this target. This finding could mean the discovery of a new allosteric binding site within the transporter, which could lead to development of a new class of compounds with increased potency and specificity at Sx_c^-.

Chapter 2. Neurochemistry International Publication

NOVEL DI-ARYL-SUBSTITUTED ISOXAZOLES ACT AS NONCOMPETITVE INHBIITORS OF THE SYSTEM X_C^- GLUTAMATE CYSTINE EXCHANGER

J. Newell, C.M. Keyari, P. Diaz, N.R. Natale, S. A. Patel, R. J. Bridges*

Center for Structural & Functional Sciences, Department of Biomedical & Pharmaceutical Sciences, Skaggs School of Pharmacy, University of Montana, Missoula, MT, 59812

Corresponding Author

Department of Biomedical & Pharmaceutical Sciences

University of Montana

32 Campus Dr.

Missoula, MT 59812-1552

richard.bridges@umontana.edu

ABSTRACT

The System X_C^- antiporter is plasma membrane transporter that mediates the exchange of extracellular L-cystine with intracellular L-glutamate. This exchange is significant within the context of the CNS because the import of L-cystine is required for the synthesis of the antioxidant glutathione, while the efflux of L-glutamate has the potential to contribute to either excitatory signaling or excitotoxic pathology. Changes in the activity of the transport system have been suggested to contribute to the underlying pathological mechanisms of a variety of CNS disorders, one of the most prominent of which is it highly enriched expression glial brain tumors. In an effort to produce more potent System X_C^- blocker, we have been using amino-3-carboxy-5-methylisoxazole propionic acid (ACPA) as a scaffold for inhibitor development. We previously demonstrated that the addition of lipophilic aryl groups to either the #4 or #5 position on the isoxazole ring markedly increased the inhibitory activity at System X_C^-. In the present work a novel series of analogues has been prepared in which aryl groups have been introduced at both the #4 and #5 positions. In contrast to the competitive action of the mono-substituted analogues, kinetic analyses indicate that the di-substituted isoxazoles block System X_C^--mediated uptake of ^{3}H-L-glutamate into SNB-19 activity by a noncompetitive mechanism. These new analogues appear to be the first noncompetitive inhibitors identified for this transport system, as well as being among the most potent blockers identified to date. These diaryl-isoxazoles should be of value in assessing the physiological roles and molecular structure of System X_C^-.

19

1. INTRODUCTION

The System X_C^- (Sx_c^-) antiporter is a plasma membrane transporter present in multiple cell types that typically mediates the exchange of extracellular L-cystine (L-Cys$_2$) with intracellular L-glutamate (L-Glu) (for review see: (Bridges *et al.*, 2012a; Bridges *et al.*, 2012b; Lewerenz *et al.*, 2013). Functioning as an obligate exchanger, the antiporter utilizes the L-Glu concentration gradient generated by the Na-dependent excitatory amino acid transporters (EAATs) to drive the uptake of L-Cys$_2$. Once inside the cell, the L-Cys$_2$ is rapidly reduced to L-cysteine (L-CysH) where, among many metabolic roles, it serves as a rate-limiting precursor in the synthesis of the glutathione. While studies in most cells have focused on the role of Sx_c^- in glutathione production and antioxidant protection, the requisite efflux of L-Glu through the antiporter carries with it added significance in the CNS, where this L-Glu has the potential to contribute to both excitatory signaling and excitotoxic pathology. When both the import of L-Cys$_2$ and the export of L-Glu are taken into account, the Sx_c^- antiporter has been linked to a very wide array of physiological and pathological processes including: brain tumor growth (Watkins *et al.*, 2012), drug addiction (Madayag *et al.*, 2010; Reissner *et al.*, 2010), chemosensitivity and chemoresistance (Huang *et al.*, 2005), viral pathology (Espey *et al.*, 1998), oxidative protection (Shih *et al.*, 2006), the operation of the blood brain barrier (Hosoya *et al.*, 2002), neurotransmitter release (Baker *et al.*, 2002), and synaptic organization (Augustin *et al.*, 2007). Of particular interest, is the role of Sx_c^- in gliomas, where astrocytoma cells express markedly enriched levels of Sx_c^- and the obligate export of L-Glu that accompanies the import of Cys$_2$ (possibly to meet the increased synthetic demands for GSH) appears large enough to produce an excitotoxic necrosis that may aid

20

tumor growth, migration and the production of peritumoral seizures (Lyons *et al.*, 2007; Patel *et al.*, 2004; Sontheimer, 2008; Ye *et al.*, 1999). Significantly, the development of more potent and selective blockers of Sx_c^- hold considerable potential to suppress the growth of primary brain tumors(Sontheimer *et al.*, 2012).

Sx_c^- is a eukaryotic <u>H</u>eteromeric <u>A</u>mino acid <u>T</u>ransporter (HAT) (*aka* glycoprotein-associated amino acid exchangers) classified within the <u>A</u>mino acid, <u>P</u>olyamine, and organic <u>C</u>ation (APC) transporter super-family and <u>L</u>-<u>A</u>mino acid <u>T</u>ransporter (LAT) family (Palacin *et al.*, 2005; Verrey *et al.*, 2004). As the HAT classification suggests, Sx_C^- is composed of a glycoslated "heavy chain" required for the trafficking and cell surface expression of the dimer (4F2hc *aka* CD98, SLC3 family) and a "light chain" that mediates transport activity (xCT, SLC7A11). Structural studies on the xCT subunit indicate that it possesses 12 transmembrane domains (TMDs), intracellular N and C termini, and a reentrant loop between TMD 2 and 3 that may participate in substrate binding and translocation (Gasol *et al.*, 2004; Jimenez-Vidal *et al.*, 2004). While physiologically Sx_C^- mediates the exchange of intracellular L-Glu and extracellular L-Cys_2, its activity can be followed by quantifying the uptake of either radiolabeled substrate, with each acting as a competitive inhibitor of the other. When compared to the EAATs, Sx_C^- exhibits a distinct ionic dependency (Cl-dependent, Na-independent) and pharmacological specificity (Bridges *et al.*, 2012b). Unfortunately, many of compounds initially identified as inhibitors of Sx_C^- are also well known for interacting with other components of the EAA system (e.g., quisqualate, ibotenate, serine-O-sulfate and bromo-homo-ibotenate), decreasing their utility for functional studies in more complex

physiological preparations. For these reasons we have been pursuing the development of more potent and selective inhibitors of Sx_C^-.

Not withstanding the issue of cross-reactivity, the actions of the isoxazoles and closely related heterocyclics mentioned above prompted the development of a series of derivatives based upon amino-3-carboxy-5-methylisoxazole propionic acid (ACPA). While ACPA exhibits little or no activity itself, the systematic addition of lipophilic substituents onto its isoxazole ring has yielded a growing library on increasingly potent Sx_C^- inhibitors (Matti *et al.*, 2013; Patel *et al.*, 2010). The more effective inhibitors within this series included the introduction of benzyl or naphthyl-based aryl groups at two positions on the isoxazole ring: *i*) replacing the methyl moiety at position #4 or, *ii*) via a hydrazone linkage, replacing the ethyl amino acid group at position #5. In all cases kinetically examined in detail, the analogues acted as competitive blockers of the Sx_C^--mediated uptake of ^{3}H-L-Glu, leading to the conclusion that there were lipophilic domains adjacent to the substrate binding site on the transport protein. To further assess the relative position of these lipophilic domains, several 4,5-di-substituted ACPA derivatives were prepared to test whether the aryl groups were interacting with one or two distinct sites (Patel *et al.*, 2010). While considerably less active as Sx_C^- inhibitors than a number of the mono-substituted isoxazoles, the results nonetheless were consistent with the presence of two lipophilic "pockets" on the antiporter. In the present work we have continued optimizing aryl group substituents at the 4 and 5 positions of the isoxazole ring of the ACPA template to generate some of the most potent inhibitors of Sx_C^- yet identified. Further, kinetic analyses indicate that unlike the parent mono-substituted derivatives, these "hybrid" di-substituted isoxazoles act as noncompetitive inhibitors of

22

Sx_C^-. These findings identify a new pharmacological strategy with which to regulate Sx_C^- activity, as well as raise interesting questions as to the position of the lipophilic domains relative to the substrate binding site on the transporter.
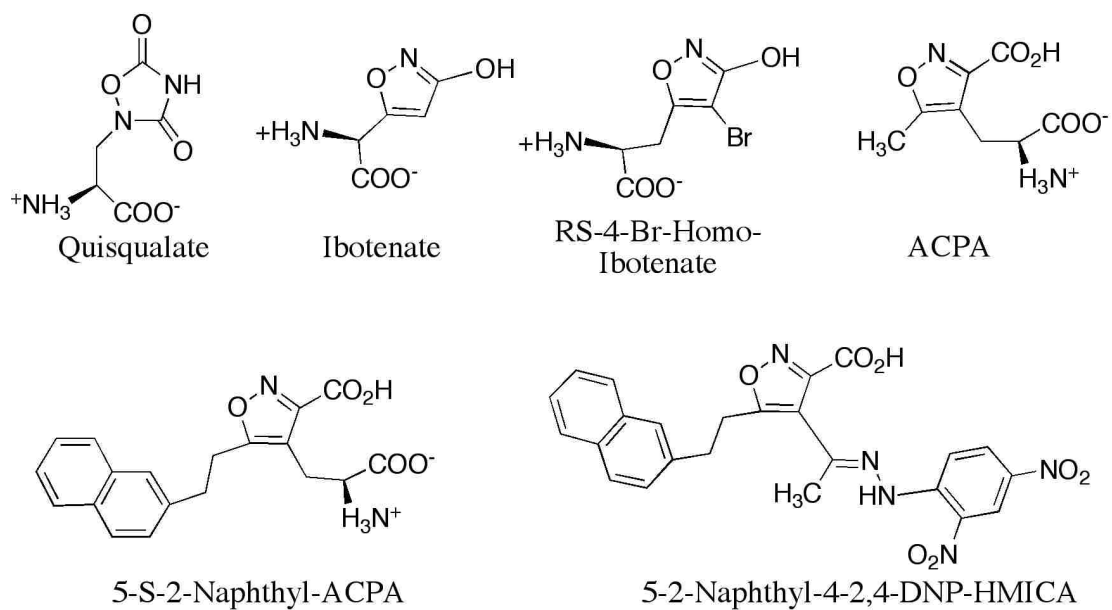
2. METHODS AND MATERIALS

2.1 Chemistry: Synthesis

The novel analogues reported in this study were prepared from the bromo acetal **6** shown in **Scheme 2.1** (Nelson *et al.*, 2008). Suzuki-Miyaura palladium (McDaniel *et al.*, 2011) catalyzed coupling with the corresponding arylboronic acids put the C-5 aryl in place, **7-9**, hydrolysis of the acetal, hydrazone condensation (Patel *et al.*, 2010), and hydroylsis of the C-3 ester under basic conditions (Matti *et al.*, 2013) to arrive at the products **2-4** was then accomplished as previously described.
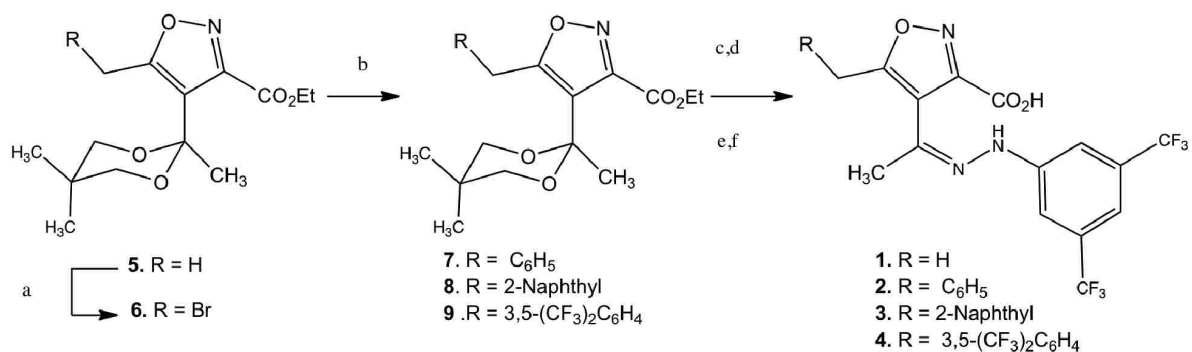
2.2 Cell Culture

SNB-19 glioma cells, purchased from American Type Culture Collection (Manassas, VA), were grown in DMEM/F-12 medium (pH 7.4) containing 1 mM pyruvate and 16 mM $NaHCO_3$ and supplemented with 10% fetal calf serum. The cells were cultured in 150 cm^2 flasks (Corning) and maintained at 37 °C in a humidified atmosphere of 5% CO_2. In the $[^3H]$-L-glutamate uptake experiments, cells were seeded in 12 well culture plates (Costar) at a density of 5 x 10^4 cells/well and maintained for 3 days until 80-90% confluent. Protein concentrations were determined by the bicinchoninic acid (BCA) method (Pierce).

Figure 2.1: Structures of Isoxasole-Based Ligands

Quisqualate

Ibotenate

RS-4-Br-Homo-
Ibotenate

ACPA

5-S-2-Naphthyl-ACPA

5-2-Naphthyl-4-2,4-DNP-HMICA

Scheme 2.1: Reagents and Reaction Conditions

5. R = H
6. R = Br

7. R = C₆H₅
8. R = 2-Naphthyl
9. R = 3,5-(CF₃)₂C₆H₄

1. R = H
2. R = C₆H₅
3. R = 2-Naphthyl
4. R = 3,5-(CF₃)₂C₆H₄

Reagents and reaction conditions: a. NBS CCl₄ b. ArB(OH)₂, PdL₄, CsCO₃ c TsOH,

Acetone d. Bis-3,5-trifluoromethylphenylhydrazine e. 3N NaOH f. HCl

2.3 Glutamate Uptake Assay

Uptake of ^{3}H-L-glutamate into cultured cells was quantified using a modification of the procedure of Martin and Shane as previously described Patel et al., 2010. Briefly, individual wells after removal of culture media, were rinsed three times and pre-incubated in 1 ml Na$^+$-free HEPES buffered (pH 7.4) Hank's balanced salt solution (HBHS) at 30 °C for 5 min. The Na$^+$-free buffer contained: 137.5 mM choline Cl, 5.36 mM KCl, 0.77 mM KH_2PO_4, 0.71 mM $MgSO_4.7H2O$, 1.1 mM $CaCl_2$, 10 mM D-glucose, and 10 mM HEPES. Uptake was initiated by aspiration of the pre-incubation buffer and the addition of a 500 ml aliquot of Na$^+$-free transport buffer containing ^{3}H-L-glutamate (4–16 mCi/ml) mixed with L-glutamate (10–500 mM, final concentration). In those assays that evaluated inhibitor activity, the 500 ml aliquot of transport buffer contained both the ^{3}H-L-glutamate and potential inhibitors to ensure simultaneous addition. Following a 5 min incubation at 30 °C, the assays were terminated by three sequential 1 ml washes with ice cold buffer and then the cells were dissolved in 1 ml of 0.4 M NaOH for 24 h. An aliquot (200 ml) was then transferred into a 5 ml glass scintillation vial and neutralized with the addition of 5 ml glacial acetic acid followed by 3.5 ml Liquiscint@ scintillation fluid (National Diagnostics) to each sample. Incorporation of radioactivity was quantified by liquid scintillation counting (LSC, Beckman LS 6500). Values are reported as mean ± S.E.M and are corrected for non-specific uptake (e.g., leakage and binding) by subtracting the amount of ^{3}H-L-glutamate accumulation at 4°C.

2.4 Kinetic Analyses

Michaelis-Menten and Lineweaver–Burk plots and associated kinetic parameters (K_m and V_{max}) for transport inhibitors were estimated using a non-linear curve fitting analysis

(KaleidaGraph 3.6.5). K_i determinations from LWB and Eadie-Hofstee replots were calculated using linear-regression analysis (KaleidaGraph 3.6.5).

3. RESULTS

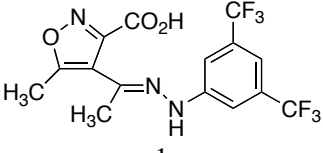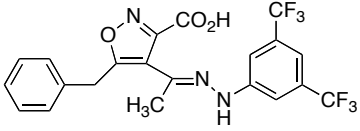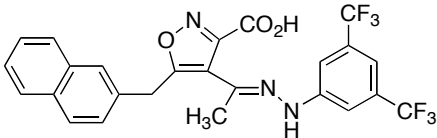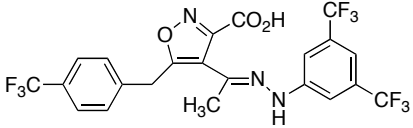### 3.1 Inhibition of the Sx_c^--mediated uptake of ^{3}H-L-glutamate

The inhibitory activity of the compounds was determined by quantifying the ability of the analogues to reduce the accumulation of ^{3}H-L-Glu into human SNB-19 glioblastoma cells under Cl-dependent (Na-free) conditions. A number of glioma cell lines, including SNB-19, express markedly higher levels of Sx_c^- and reduced levels of the sodium-dependent excitatory amino acid transporters (EAATs) than do primary astrocytes, making them well suited for pharmacological assays of the exchanger (Ye *et al.*, 1999). The compounds were initially screened at a single concentration of substrate (100 µM ^{3}H-L-Glu) and isoxazole (500 µM) to confirm to inhibitory activity. As reported in Table 1, all of the analogues almost completely blocked the uptake of the ^{3}H-L-Glu in to cells. (The data are reported as % of control uptake, thus the smaller the number the greater the level of inhibition.) The activity for 4-bis-TFM-HMICA (Compound #1, Table 1) has been previously reported, although its kinetic mechanism had not been examined in detail (see below). These initial screenings confirmed that the introduction of aryl groups to isoxazole scaffold as both mono-substitutions at the 4 or 5 positions or di-substitutions at both could produce potent inhibitors of Sx_c^-.

### 3.2 Competitive Inhibition of the Sx_c^- by the mono-substituted isoxazoles

The inhibitory action of 4-bis-TFM-HMICA was characterized in greater detail using a standard Michaelis-Menten analysis in which the concentration of both the isoxazole

derivative and substrate (^{3}H-L-Glu) were systematically varied. While the inhibitory activity of 4-bis-TFM-HMICA has been previously reported, that study did not include a characterization of it kinetic mechanism. A representative series of plots from of these assays are depicted in Figure 2, which includes both a V *vs*. S plot (Panel A) and a 1/V *vs*. 1/S Lineweaver-Burk plot (Panel B). The pattern of inhibition displayed by 4-bis-TFM-HMICA is representative of a competitive mechanism and is consistent with the inhibitory action of related isoxazoles that have been modified with aryl groups at the C4 position of the heterocyclic ring (Matti *et al.*, 2013; Patel *et al.*, 2010). A replot of the slopes of the lines from the representative Lineweaver-Burk plot *vs*. [I] (Figure 2, Panel C) was used to determine K_i. An average of n=3 such analyses yielded a K_i of 61 ± 5 μM for 4-bis-TFM-HMICA (Table 1). A replot of averaged $K_{m,apparent}$ vs. [I] was also linear and yielded a similar K_i value (≈ 80 μM), as would be expected for a competitive inhibitor (plot not shown) (Segel, 1993).

**Table 2.1: Percent of Control Uptake of ^{3}H-L-Glu and K$_i$ Values for Sx$_c^-$**

Compound (500 μM)	Sx$_c^-$-mediated ^{3}H-L-Glu uptake (% of Control)	Ki Value from LWB Slope Replots	Inhibitory Mechanism
1 (Z)-4-(1-(2-(3,5-bis(trifluoromethyl)phenyl)hydrazono)ethyl)-5-methylisoxazole-3-carboxylic acid ***4-bis-TFM-HMICA***	14 ± 4 (n=3)	61 ± 5 μM (n=3)	Competitive
2 (Z)-5-benzyl-4-(1-(2-(3,5-bis(trifluoromethyl)phenyl)hydrazono)ethyl)isoxazole-3-carboxylic acid ***5-Benzyl-4-bis-TFM-HMICA***	6 ± 1 (n=3)	22 ± 2 μM (n=3)	Noncompetitive
3 (Z)-4-(1-(2-(3,5-bis(trifluoromethyl)phenyl)hydrazono)ethyl)-5-(naphthalen-2-ylmethyl)isoxazole-3-carboxylic acid ***5-Naphthyl-4-bis-TFM-HMICA***	14 ± 4 (n=3)	13 ± 1 μM (n=3)	Noncompetitive
4 (Z)-4-(1-(2-(3,5-bis(trifluoromethyl)phenyl)hydrazono)ethyl)-5-(4-(trifluoromethyl)benzyl)isoxazole-3-carboxylic acid ***5-4-TFM-Benzyl-4-bis-TFM-HMICA***	6 ± 9 (n=5)	3 ± 1 μM (n=5)	Noncompetitive

Figure 2.2: Representative Kinetic Analyses and K_i Determination for

4-bis-TFM-HMICA
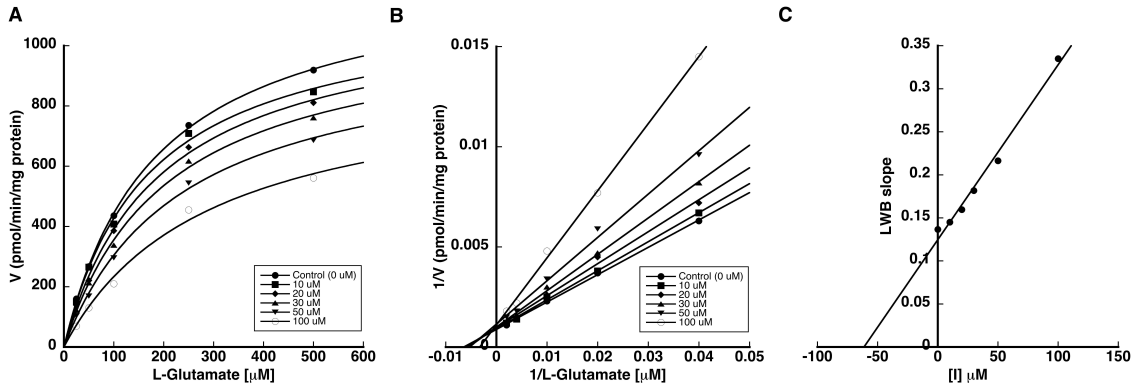
SNB-19 cells were assayed for ^{3}H-L-Glutamate uptake under Cl-dependent (Na-free) conditions in the presence of a range of inhibitor concentrations. Data are plotted as pmol/min/mg protein and have been corrected for non-specific uptake and leakage. Panels A and B, K_m (=150 µM) and V_{max} (=1100 pmol/min/mg protein) values were determined by non-linear curve fitting of the saturation curves and linear regression analysis of LWB plots (KaleidaGraph 4.1.3). Panel C, K_i (70 µM) values were determined by linear regression of LWB slope vs. [I] replot.

Figure 2.3: Representative Kinetic Analysis of 5-4-TFM-Benzyl-4-bis-TFM-HMICA

Displaying Noncompetitive Inhibition
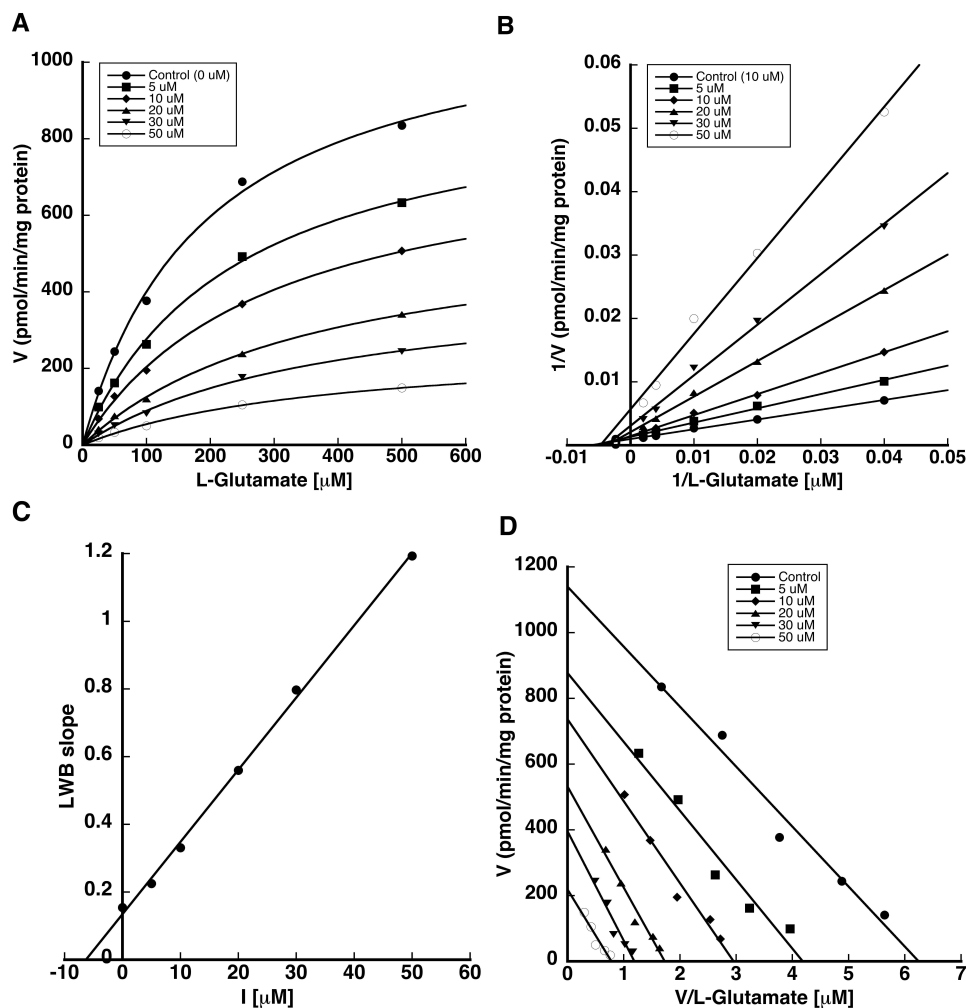
Panel A, Michaelis-Menten analysis. Panel B, LWB replot. Panel C, LWB slope vs. [I] replot. Panel D, Eadie-Hofstee replot. K_m ($\approx$ 160 μM), V_{max} ($\approx$1100 pmol/min/mg protein), and K_i (3 μM) values for plots shown were determined using KaleidaGraph 4.1.3.

3.3 Noncompetitive Inhibition of the Sx_c^- by di-substituted isoxazoles

The di-substituted isoxazole analogues with aryl groups appended at both the #4 and #5 position were similarly assayed to determine a mechanism of inhibition. Representative plots are shown in Figure 3 for 5-4-TFM-Benzyl-4-bis-TFM-HMICA (Compound #4, Table 1), the most potent of the blockers examined. In contrast to mono-substitutions made at either of these positions, all three di-substituted analogues exhibited a pattern of inhibition consistent with noncompetitive inhibitors. Both the V *vs*. S and Lineweaver-Burk plots demonstrate that the inhibitors produced a decrease in V_{max} with little or no change in K_m, as would be expected of noncompetitive inhibition. Again, replots of the slopes from the Lineweaver-Burk graphs were linear and used to determine K_i values (Table 1). A representative slope replot for 5-4-TFM-Benzyl-4-bis-TFM-HMICA is included in Figure 3, Panel C (average $K_i = 3 \pm 1$ µM, n=5). Competitive and noncompetitive inhibitors can also be distinguished by replots from Lineweaver-Burk graphs of either $K_{m,apparent}$ vs. [I], linear for competitive mechanisms, or $1/V_{max, apparent}$ vs. [I], linear for noncompetitive inhibition (Segel, 1993). In the instance of 5-4-TFM-Benzyl-4-bis-TFM-HMICA, the replot of $1/V_{max, apparent}$ vs. [I] was indeed linear and yielded a K_i of ≈ 8µM (plots not shown). If both the slope replot and the $1/V_{max, apparent}$ vs. [I] replot yield similar K_i values, as is the case for 5-4-TFM-Benzyl-4-bis-TFM-HMICA, the analogue is considered to be acting as a "pure" noncompetitive inhibitor, where the binding of the inhibitor does not alter the binding affinity of the substrate (Segel, 1993). Interestingly, while the K_i values determined by these two replot methods for 5-4-TFM-Benzyl-4-bis-TFM-HMICA and 5-Naphthyl-4-bis-TFM-HMICA (Compound #3, Table 1) were not markedly different, the K_i values for 5-Benzyl-4-bis-TFM-HMICA

(Compound #2, Table 1) generated from the $1/V_{max,apparent}$ vs. [I] replots was $\approx 60\ \mu M$ (average n=3), a substantial increase over the $\approx 20\mu M\ K_i$ determined by the slope replot method (plots not shown). This would suggest that in contrast to the other noncompetitive inhibitors, the binding of 5-Benzyl-4-bis-TFM-HMICA to Sx_c^- also decreased the affinity with which the transporter binds L-Glu.

As the identification of the di-substituted isoxazoles as noncompetitive inhibitors was unexpected, the kinetic data was also analyzed using the Eadie-Hofstee method as a second graphical approach. As depicted in Figure 3 (Panel D) for 5-4-TFM-Benzyl-4-bis-TFM-HMICA, the plots of V *vs.* V/[S] for it and 5-Naphthyl-4-bis-TFM-HMICA yielded a series of parallel lines, a pattern indicative of noncompetitive inhibition. The Eadie-Hofstee plot for 5-Benzyl-4-bis-TFM-HMICA generated non-intersecting lines consistent with mixed inhibition (plot not shown). This pattern of mixed inhibition is consistent with the analysis described above in which the binding of the inhibitor also reduces the ability of the transporter to bind L-Glu as a substrate. When the K_m/V_{max} (equivalent to a Lineweaver-Burk slope) and $1/V_{max,apparent}$ values garnered from the Eadie-Hofstee graphs were replotted *vs.* [I], the resulting K_i values were very similar to those determined from replots of the Lineweaver-Burk graphs (plots not shown).

4. DISCUSSION

To the best of our knowledge, the diaryl-substituted isoxazoles described here represents the first noncompetitive blockers to be indentified for the Sx_c^- transport system. This mechanism of action was not anticipated, as these compounds emerged during the course of structure-activity-relationship (SAR) studies aimed at the optimization of rationally

designed competitive inhibitors. Thus, the isoxazole scaffold was selected for analogue development because of the previously characterized inhibitory activity of a number of closely related compounds, including quisqualate, ibotenate, and bromo-homoibotenate (Bridges *et al.*, 2012b). Employing amino-3-carboxy-5-methylisoxazole (ACPA) as a starting point, it was found that the inhibitory activity increased as aryl groups were systematically introduced at either the 5 position on the isoxazole ring (replacing the methyl group on ACPA) or the 4 position of the isoxazole via a hydrazone linkage (replacing a-amino acid moiety) (Matti *et al.*, 2013; Patel *et al.*, 2010). Of these derivatives, S-2-naphthyl-ethyl-ACPA emerged as one of the more potent Sx_c^- inhibitors. Detailed kinetics analysis similar to those employed in the present study confirmed that it competitively inhibited the Sx_c^--mediated uptake of ^{3}H-L-Glu into SNB-19 cells with a K_i of about 50 µM (Patel *et al.*, 2010). Given the structural similarities between the analogues, it was assumed at that time that 4-bis-TFM-HMICA, in which the aryl substitution was made at the 4 position of the isoxazole ring was also acting as a competitive manner. That this was indeed the case is confirmed in the present report, where Michaelis-Menten and Lineweaver-Burk analyses demonstrated it competitively inhibited the uptake of ^{3}H-L-Glu into SNB-19 cells with a K_i of about 60 µM. The results also confirm the utility and potency of 4-substituted aryl isoxazole as inhibitors. These SAR data were particularly valuable, as the results suggest that there are lipophilic pockets adjacent to the substrate binding site on Sx_c^- and that the presence of these domains can be exploited, much in the same manner as has been done with the excitatory amino transporters (EAATs) (Bridges R, 2009), to develop more potent and specific inhibitors.

SAR-based comparisons between the 4- and 5-aryl substituted isoxazole raised intriguing questions as to whether the aryl groups were interacting with the same domains on the transporter (necessitating a change in the manner in which the isoxazole ring was accommodated) or that there are two distinct lipophilic domains present on Sx_c^-. This issue was directly addressed through the synthesis and testing of comparable isoxazoles that were modified at both positions. Although markedly less potent than the mono-substituted isoxazoles, the ability of these first "hybrid" analogues to also block the Sx_c^--mediated uptake of ^{3}H-L-Glu into SNB-19 cells supported the conclusion that there were at least two distinct lipophilic domains on the transporters, although the mechanism of inhibition remained to be elucidated (Patel *et al.*, 2010). These results prompted the optimization of the di-substituted isoxazoles and the preparation of the three analogues characterized in the present study. As initial screening assays suggested that these new isoxazoles were among the best inhibitors yet developed for Sx_c^- (Table 1), kinetic studies were carried out to determine K_i values. Surprisingly, the Michaelis-Menten and Lineweaver-Burk analyses of the concentration dependence with which the di-substituted isoxazoles inhibited the Sx_c^--mediated uptake of ^{3}H-L-Glu into SNB-19 cells revealed a noncompetitive mechanism rather than a competitive one. Similarly, when the uptake rates were analyzed using Eadie-Hofstee plots as a second approach, the resulting pattern of lines was again indicative of a noncompetitive inhibitor. The Lineweaver-Burk plots were further analyzed by repotting both the slope and $1/_{Vmax, apparent}$ ($1/V_{intercept}$) vs. [I]. If a compound is acting as "pure" noncompetitive inhibitor, then these two replots should both be linear and yield the same value for K_i (i.e., -X intercept). This was the case for 5-4-TFM-Benzyl-4-bis-TFM-HMICA, where its K_i value of about 5 μM places it among

35

the most potent Sx_c^- inhibitors yet identified (Bridges *et al.*, 2012b). Mechanistically, the data suggest this inhibitor can bind to either the empty or substrate-occupied transporter to produce a "dead end" complex (i.e., an inactive transporter) and that is does so in a manner that does not alter the binding of the substrate (e.g., L-Glu). Among the three isoxazoles examined, only 5-Benzyl-4-bis-TFM-HMICA exhibited a substantial difference between the two replots methods, yielding a K_i of about 20 µM from the slope replot and 60 µM from the 1/V intercept replot. While there are different types of mixed inhibition involving multiple sites of interaction that could produce such results, the most straightforward interpretation suggests that 5-Benzyl-4-bis-TFM-HMICA is noncompetitively inhibiting Sx_c^- with a K_i of ≈20 µM, but that when it is bound the analogue also reduces the affinity of the transporter for its substrate (Segel, 1993). Such a interpretation is also supported by the fact that the other closely related di-substituted isoxazoles are both more potent and act as "pure" noncompetitive inhibitors.

The switch from a competitive to a noncompetitive mechanism observed with the di-substituted isoxazoles raises intriguing questions as to the molecular relationships between the potential sites of action on Sx_c^-. Based upon the competitive action of the mono-substituted isoxazoles, such as 4-bis-TFM-HMICA, it was hypothesized that the isoxazole portion of the molecule was acting as an L-Glu mimic and interacting with substrate binding domains, while the trifluoromethyl-substituted benzyl group was interacting with an adjacent lipophilic domain. As a consequence of occupying some portion of the substrate site, it would competitively block the binding of L-Glu. The 5-monosubstituted isoxazole would be hypothesized to bind in an analogous manner, only it would be interacting with a different lipophilic domain, the presence of which is
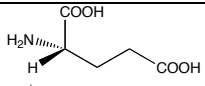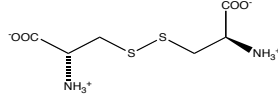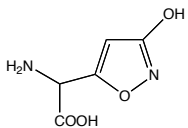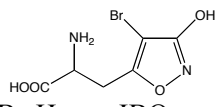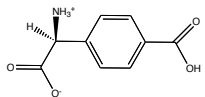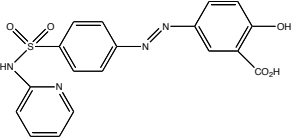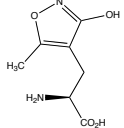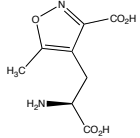
36

supported by the inhibitory action of the di-substituted "hybrid" isoxazoles. If this is

occurring, the present demonstration of the noncompetitive action of the di-substituted

analogue may reflect the optimal binding of the two aryl groups to their respective

lipophilic domains in a manner that still inhibits uptake, but also repositions the isoxazole

ring such that it is no longer directly precludes the binding of L-Glu. This, in turn, would

lead to the hypothesis that the substrate binding and lipophilic domains are located in

close proximity to one another. The competitive action of the other isoxazoles would

also be consistent with this model.   Further, lipophilic domains have been identified in a

number of other transport systems that are in close proximity to the substrate binding

domains, including the EAATs and the serotonin transport (SERT) (Bridges R, 2009;

Leary *et al.*, 2011; Zhou *et al.*, 2009). However, the possibility that the aryl-substituted

isoxazole are acting at a site well removed from the substrate binding site cannot be

excluded. In such an instance, analogue binding would have to produce conformational

changes that inhibited transport activity in a manner that may or may not have also blocks

Glu binding, reflecting competitive and noncompetitive mechanisms, respectively.

Whichever mechanisms are ultimately resolved, the marked increase in the potency of the

present inhibitors, likely also reflect the presence of the trifluoromethyl groups on the

aryl substituents. The role of fluorine in enhancing the binding affinity of the ligands

likely arises from either the proper filling of apolar pockets, multipolar C–F···H–N, C–

F···C=O, and C–F···H–Cα interactions or polar interaction with electropositive side

chains (Bissantz *et al.*, 2010; Muller *et al.*, 2007; Zhou *et al.*, 2009; Zurcher *et al.*, 2008)

}. It is entirely plausible that with three trifluoromethyl groups present on the most

potent inhibitor, 5-4-TFM-Benzyl-4-bis-TFM-HMICA, that several types of interactions

contribute to the enhanced binding affinity. Future work within this evolving library of compounds will focus on the continued optimization of these aryl group interactions. The protein domains with which these ligands interact have been postulated to represent either intermediate binding sites guiding substrate permeation (*e.g.*, "vestibule sites") or potential allosteric regulatory sites (e.g. "halogen binding pockets") (Singh *et al.*, 2008; Zhou *et al.*, 2009). Ligands occupying these sites may prevent the transporter from accessing one or more conformational states within the alternate access mechanism that is required for substrate translocation. Ironically, this will likely include exploring different linkers between the aryl groups that now, in the face of a noncompetitive mechanism, may no longer require the inclusion of a glutamate (or cystine) mimic.

Chapter 3. Supplemental Data

Using methods described in Chapter 2, extensive pharmacokinetic analysis was performed on potential Sx_c^- inhibitors including analogues of sulfasalazine and ACPA. A subset of these compounds have been documented in previous publications by our lab (Newell *et al.*, 2013; Patel *et al.*, 2010). Supplemental data for these compounds will be presented here, along with extensive kinetic data for the remaining compounds within this class. In addition, kinetic data for the endogenous substrate, L-Cys$_2$ is presented in **Figure 3.1** to demonstrate competitive inhibition. Competitive inhibition can also be seen for the susalimod analogue, RB 553 in **Figure 3.2**. Percent of control for each compound, as well as K_I values for LWB slope replots are presented in **Table 3.1** for early inhibitors, and in **Table 3.2** for novel susalimod and isoxazole analogues.

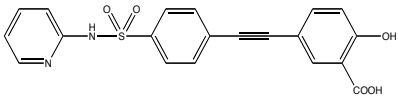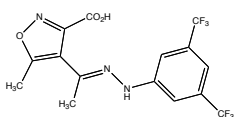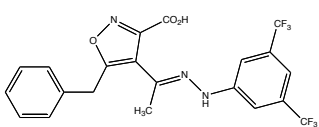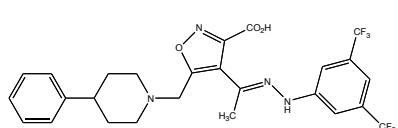**Table 3.1:** Early Inhibitors of Sx_c^-

Compound	Sx_c^- mediated ^{3}H-L-Glu Uptake (Percent of control)	K_i Values (µM)*
L-Glutamate	26 ± 3 (n=11)	
L-Cystine	22 ± 3 (n=14)	29 ± 10
Ibotenate	20 ± 1 (6)	31 ± 3
(RS)-4-Br-Homo-IBO	7 ± 1 (7)	18 ± 4
Quisqualate	1 ± 1 (n=9)	5 ± 3
(S)-4-CPG	3 ± 1 (n=3)	5 ± 1
Sulfasalazine	0.5 ± 0.5 (n=3)	
AMPA	95 ± 2 (n=6)	
ACPA	98 ± 12 (n=3)	
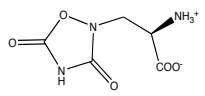
Table 3.1. Legend

For percent of control uptake of ^{3}H-L-Glu, SNB-19 cells were assayed for L-[^{3}H]-Glu (100 µM) uptake under Cl-dependent (Na-free) conditions in the presence of inhibitor (500 µM). Values are reported as mean ± SEM of control activity (accumulation in the absence of inhibitors, i.e. 100%). For K_i determination, SNB-19 cells were assayed for L-[^{3}H]-glutamate uptake in the presence of a range of inhibitor concentrations (10-500µM). K_i values were determined directly from a re-plot of Lineweaver-Burk slope vs. [I] values using linear regression fitting. Values are reported as mean ± SEM.

*For K_i values, n ≥ 3.

Table 3.2: Susalimod and Isoxasole Compounds

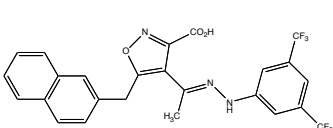| Compound	Sx_c^- mediated ^3H-L-Glu Uptake (Percent of control)	K_i from LWB slope replots	Inhibitory Mechanism
1 Susalimod	0.5 ± 0.3 (n=4)	3 ± 0.7 μM (n=4)	Competitive
2 4-bis-TFM-HMICA	14 ± 4 (n=3)	56 ± 8 μM (n=3)	Competitive
3 5-benzyl-4-bis-TFM-HMICA	6 ± 1 (n=3)	22 ± 2.5 μM (n=3)	Mixed
4 5-4-phenylpiperidinyl-4-bis-TFM-HMICA	26 ± 4 (n=3)	59 ± 9 μM (n=3)	Mixed
5 5-4-biphenyl-4-bis-TFM-HMICA	49 ± 3 (n=3)	97 ± 9 μM (n=3)	Mixed
6 5-naphthyl-4-bis-TFM-HMICA	13 ± 4 (n=5)	13 ± 1 μM (n=3)	Noncompetitive
7 5-4-TFM-benzl-4-bis-TFM-HMICA	6 ± 9 (n=5)	3 ± 1 μM (n=5)	Noncompetitive
8 5-4-methoxy-benzyl-4-bis-TFM-HMICA	4.7 ± 2.7 (n=3)	13 ± 1.6 μM (n=3)	Mixed
9 5-3-methoxy-benzyl-4-bis-TFM-HMICA	3 ± 1.7 (n=3)	37 ± 12 μM (n=5)	Mixed
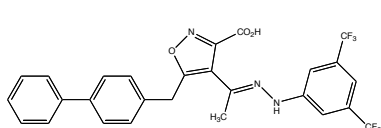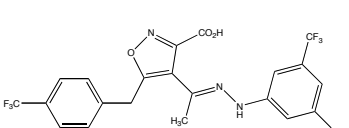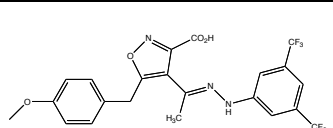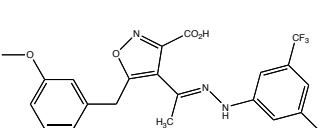
Table 3.2. Legend

For percent of control uptake of ^{3}H-L-Glu, SNB-19 cells were assayed for L-[^{3}H]-Glu (100 µM) uptake under Cl-dependent (Na-free) conditions in the presence of isoxazole-hydrazone derivatives (500 µM). Values are reported as mean ± SEM of control activity (accumulation in the absence of inhibitors, i.e. 100%). For K_i determination, SNB-19 cells were assayed for L-[^{3}H]-glutamate uptake in the presence of a range of inhibitor concentrations (10-500µM). K_i values were determined directly from a re-plot of Lineweaver-Burk slope vs. [I] values using linear regression fitting. Values are reported as mean ± SEM.

Figure 3.1: L-Cystine – Competitive Inhibition
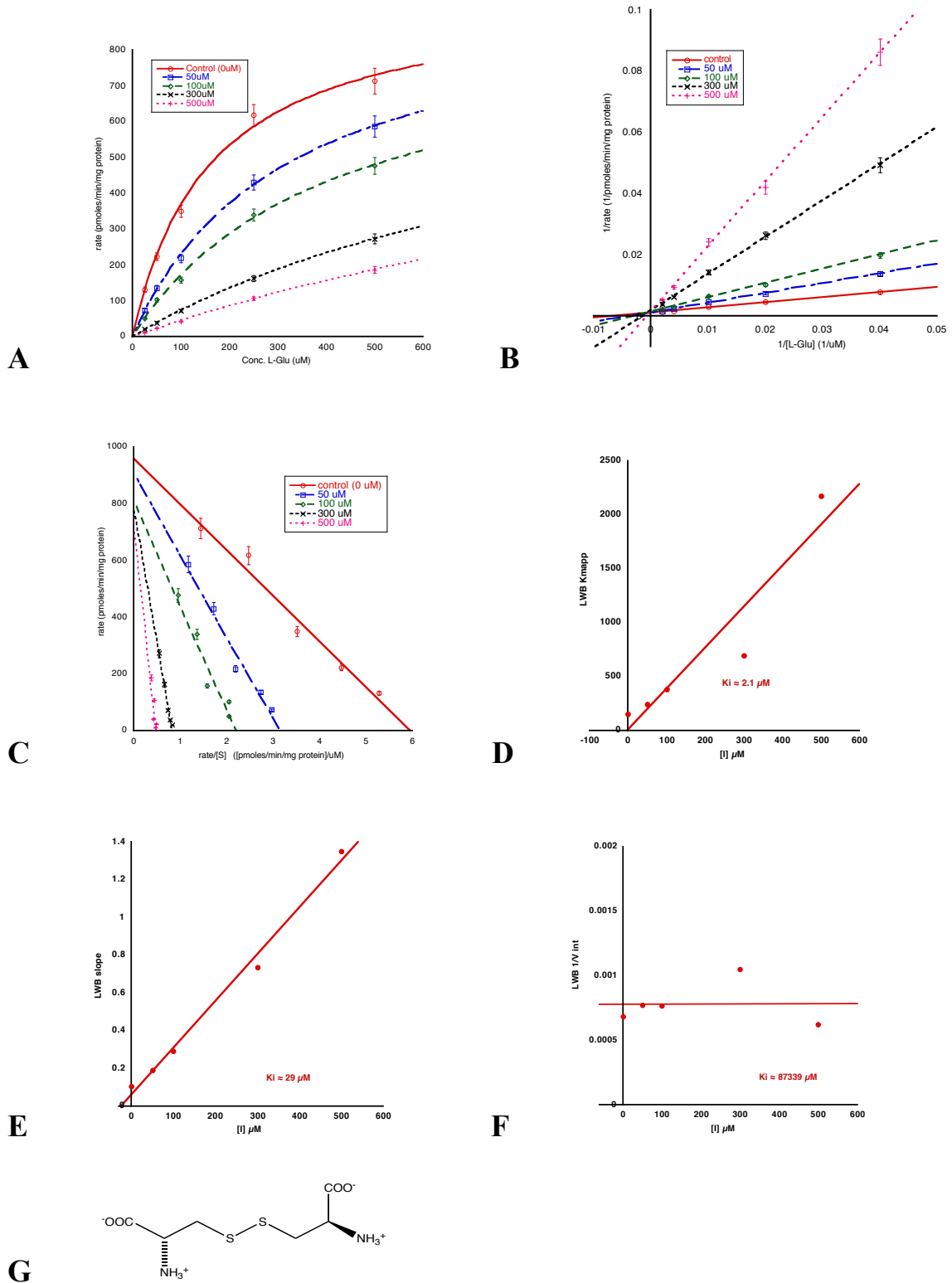
Figure 3.1. Legend

Representative kinetic analysis of L-Cystine. *Panel A*, Michaelis-Menten analysis.

Panel B, Lineweaver-Burk plot. *Panel C*, Eadie-Hofstee plot. *Panel D*, LWB $K_{m,apparent}$

vs. [I] replot. *Panel E*, LWB slope vs. [I] replot. *Panel F*, LWB $1/V_{max,apparent}$ vs. [I].

Km ($\approx$162 μM), Vmax ($\approx$ 985 pmol/min/mg protein), and Ki (29 μM) values for plots

shown were determined using KaleidaGraph (4.1.3). *Panel G,* chemical structure for L-

Cystine.

This data is consistent with competitive inhibition as seen by the constant Vmax values

and increasing $K_{m.apparent}$ values. This is represented by lines intersecting at the Y-axis for

both the LWB and Eadie-Hofstee plots. Competitive inhibition is also demonstrated by

the linear replot of $K_{m.apparent}$ vs. [I] (*panel D*).

Figure 3.2: Susalimod (**1**)– Competitive Inhibition

Figure 3.2. Legend

Representative kinetic analysis of susalimod **(1)**. *Panel A*, Michaelis-Menten analysis.

Panel B, Lineweaver-Burk plot. *Panel C*, Eadie-Hofstee plot. *Panel D*, LWB $K_{m,apparent}$

vs. [I] replot. *Panel E*, LWB slope vs. [I] replot. *Panel F*, LWB $1/V_{max,apparent}$ vs. [I].

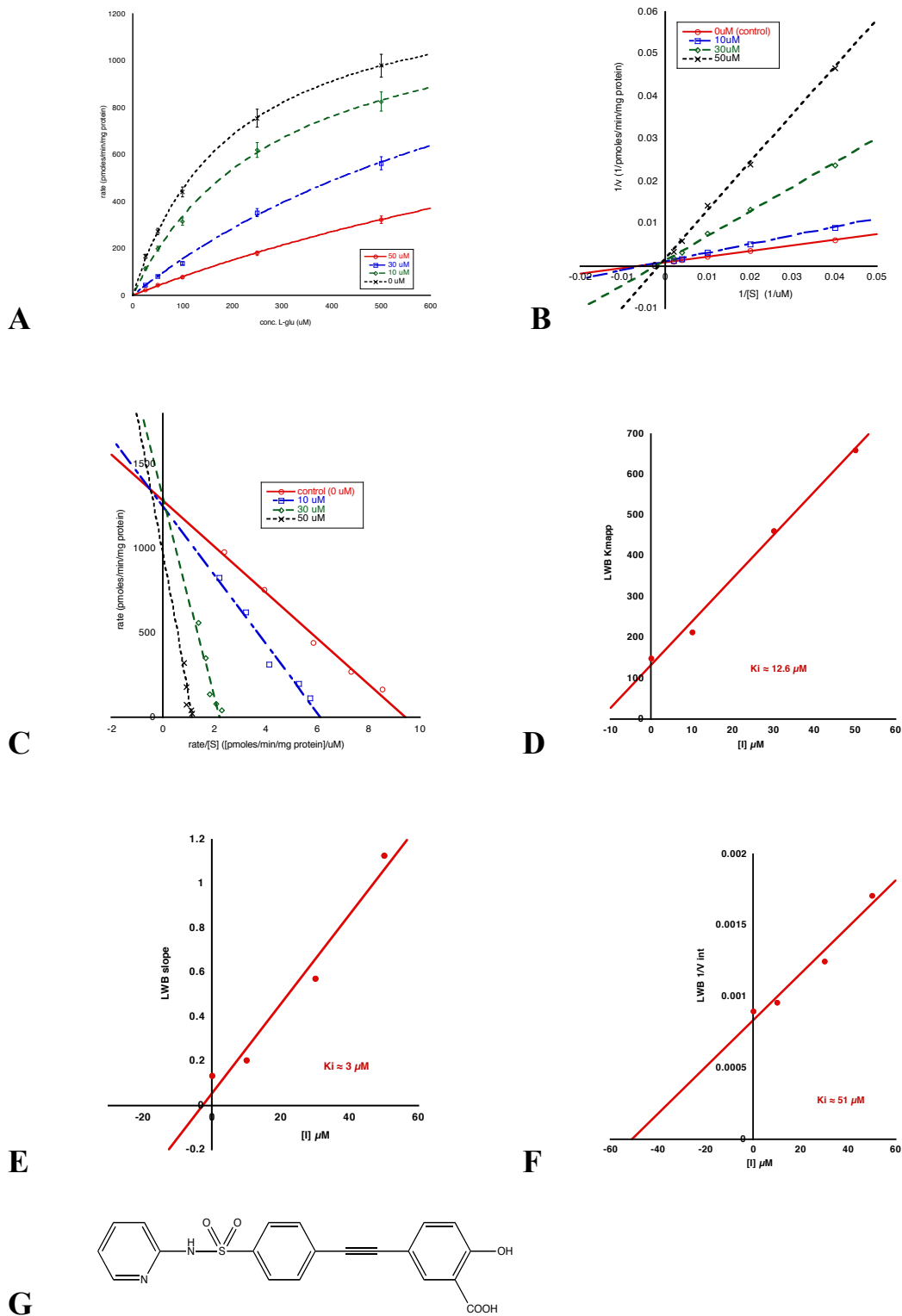Km ($\approx$205 μM), Vmax ($\approx$ 1380 pmol/min/mg protein), and Ki (3 μM) values for plots

shown were determined using KaleidaGraph (4.1.3). *Panel G,* chemical structure of

susalimod.

This data is consistent with competitive inhibition as seen by the constant Vmax values

and increasing $K_{m.apparent}$ values. This is represented by lines intersecting at the Y-axis for

both the LWB and Eadie-Hofstee plots. Competitive inhibition is also demonstrated by

the linear replot of $K_{m.apparent}$ vs. [I] (*panel D*).

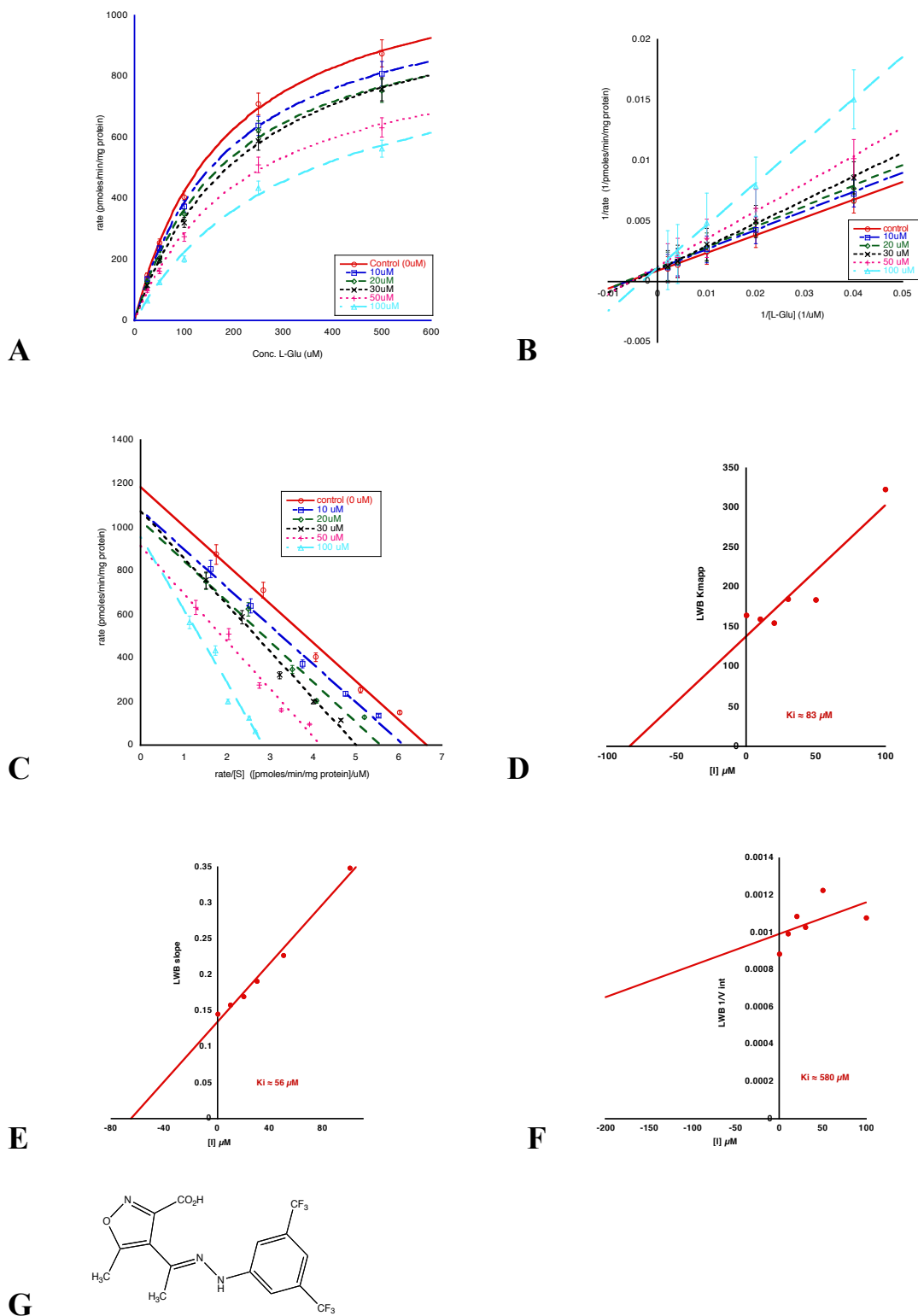**Figure 3.3:** 4-bis-TFM-HMICA (**2**) – Competitive Inhibition

Figure 3.3. Legend

Representative kinetic analysis of 4-bis-TFM-HMICA **(2)**. *Panel A*, Michaelis-Menten analysis. *Panel B*, Lineweaver-Burk plot. *Panel C*, Eadie-Hofstee plot. *Panel D*, LWB $K_{m,apparent}$ vs. [I] replot. *Panel E*, LWB slope vs. [I] replot. *Panel F*, LWB $1/V_{max,apparent}$ vs. [I]. Km ($\approx$ 188 µM), Vmax ($\approx$ 1220 pmol/min/mg protein), and Ki (56 µM) values for plots shown were determined using KaleidaGraph (4.1.3). *Panel G,* chemical structure of 4-bis-TFM-HMICA.

This data is consistent with competitive inhibition as seen by the constant Vmax values and increasing $K_{m.apparent}$ values. This is represented by lines intersecting at the Y-axis for both the LWB and Eadie-Hofstee plots. Competitive inhibition is also demonstrated by the linear replot of $K_{m.apparent}$ vs. [I] (*panel D*).

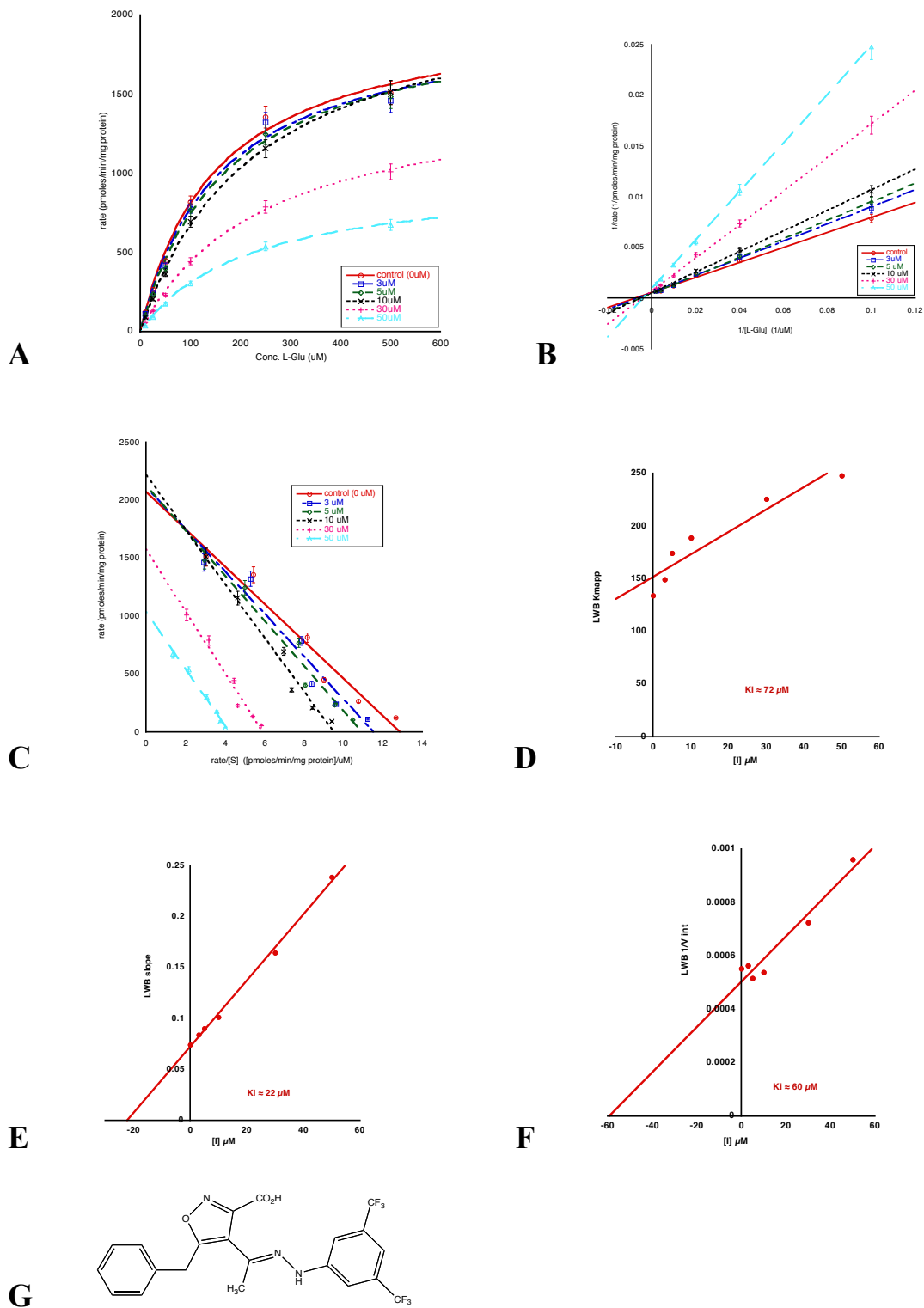**Figure 3.4:** 5-benzyl-4-bis-TFM-HMICA (**3**) – Mixed Inhibition

Figure 3.4. Legend

Representative kinetic analysis of 5-benzyl-4-bis-TFM-HMICA **(3)**. *Panel A*, Michaelis-Menten analysis. *Panel B*, Lineweaver-Burk plot. *Panel C*, Eadie-Hofstee plot. *Panel D*, LWB $K_{m,apparent}$ vs. [I] replot. *Panel E*, LWB slope vs. [I] replot. *Panel F*, LWB $1/V_{max,apparent}$ vs. [I]. Km ($\approx$ 150 μM), Vmax ($\approx$ 2040 pmol/min/mg protein), and Ki (22 μM) values for plots shown were determined using KaleidaGraph (4.1.3). *Panel G,* chemical structure of 5-benzyl-4-bis-TFM-HMICA.

These data are very difficult to interpret because it contains elements of both competitive and noncompetitive inhibition. For example, with increasing inhibitor concentrations, there is an increase in the $K_{m, apparent}$ values and a decrease in the V_{max} values. This can also be seen in the LWB plot where the lines are intersecting between the X- and Y-axes. Therefore, the mechanism of inhibition for this compound is not fully understood. In addition, since the K_i value from the $1/V_{max.apparent}$ vs. [I] is considerably higher than that of the slope vs. [I] plot, this would suggest there is a decreased affinity for which the transporter binds L-Glu.

Figure 3.5: 5-4-phenylpiperidinyl-4-bis-TFM-HMICA (**4**) – Mixed Inhibition

Figure 3.5. Legend

Representative kinetic analysis of 5-4-phenylpiperidinyl-4-bis-TFM-HMICA **(4)**. *Panel A,* Michaelis-Menten analysis. *Panel B*, Lineweaver-Burk plot. *Panel C*, Eadie-Hofstee plot. *Panel D*, LWB $K_{m,apparent}$ vs. [I] replot. *Panel E*, LWB slope vs. [I] replot. *Panel F,* LWB $1/V_{max,apparent}$ vs. [I]. Km ($\approx$ 160 μM), Vmax ($\approx$ 2000 pmol/min/mg protein), and Ki (59 μM) values for plots shown were determined using KaleidaGraph (4.1.3). *Panel G,* chemical structure of 5-4-phenylpiperidinyl-4-bis-TFM-HMICA.

These data are very difficult to interpret because panel A suggests noncompetitive inhibition while panels B and C tend to suggest more competitive inhibition. With increasing inhibitor concentrations there is also an increase in $K_{m, apparent}$ and a decrease in V_{max} observed for this compound. Therefore, the mechanism of inhibition for this compound is not fully understood. In addition, since the Ki value from the 1/Vmax.apparent vs. [I] is considerably higher than that of the slope vs. [I] plot, this would suggest there is a decreased affinity for which the transporter binds L-Glu.

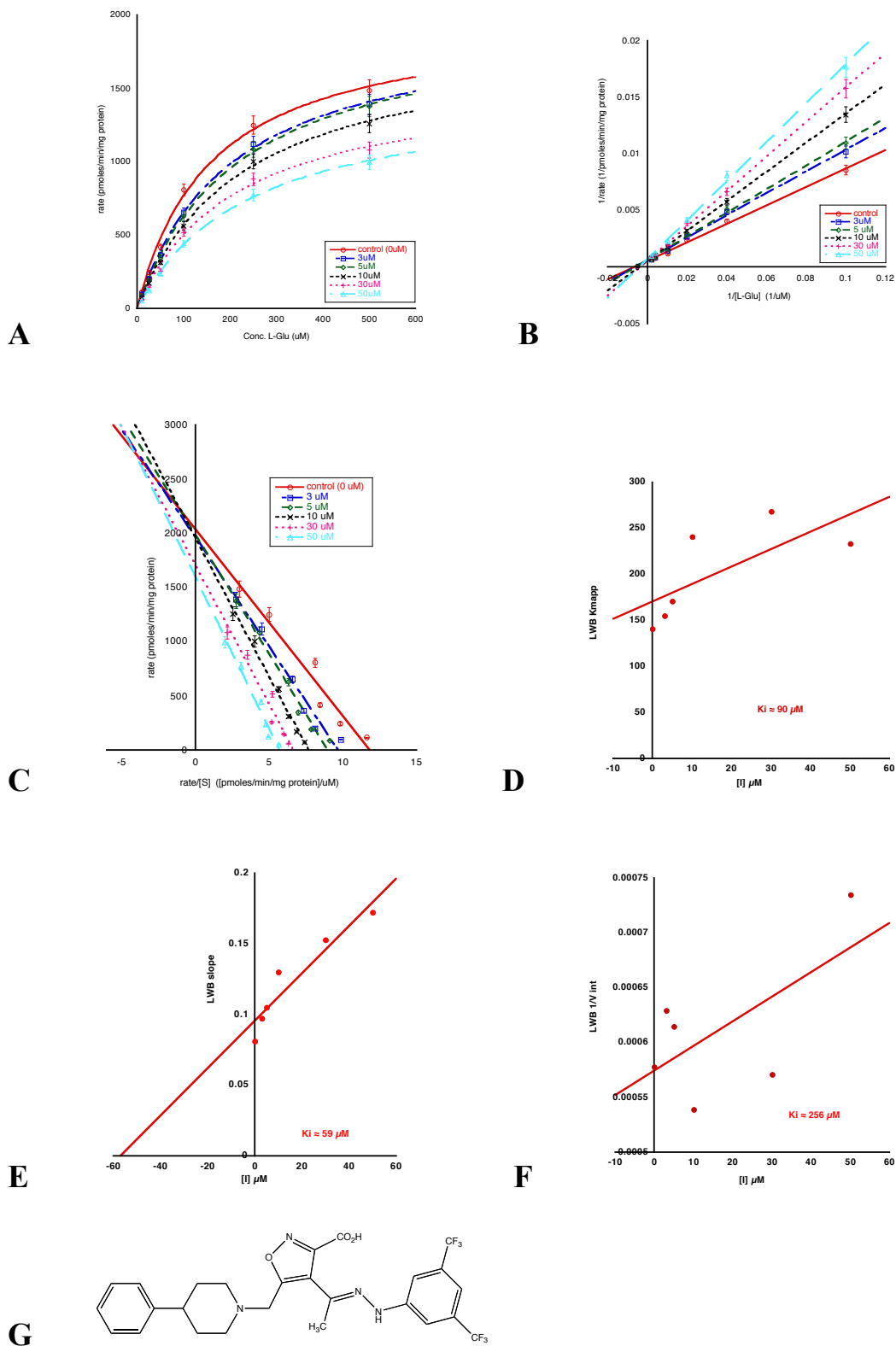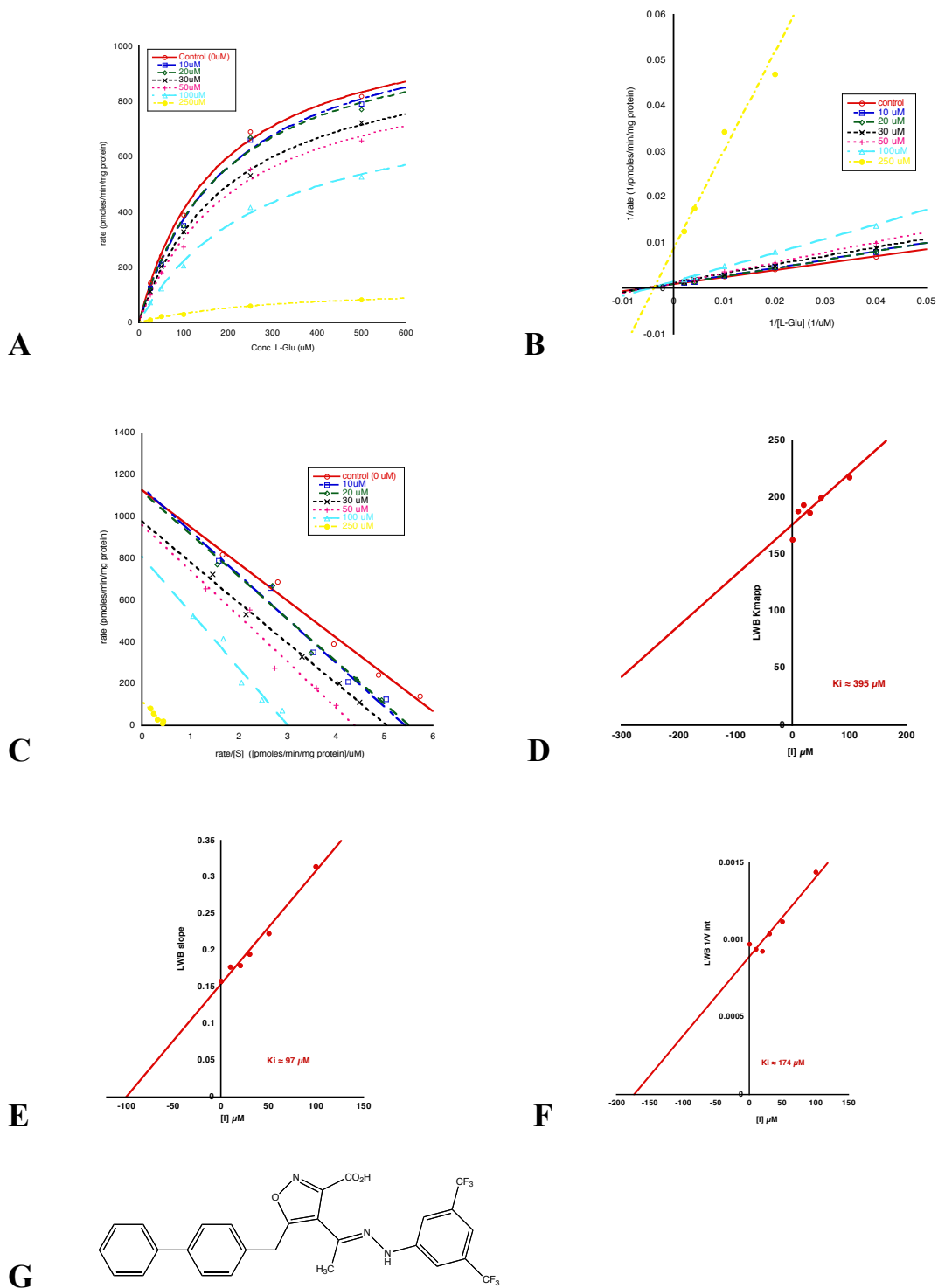**Figure 3.6:** 5-4-biphenyl-4-bis-TFM-HMICA (**5**) – Mixed Inhibition

Figure 3.6. Legend

Representative kinetic analysis of 5-4-biphenyl-4-bis-TFM-HMICA **(5)**. *Panel A*,

Michaelis-Menten analysis. *Panel B*, Lineweaver-Burk plot. *Panel C*, Eadie-Hofstee

plot. *Panel D*, LWB $K_{m,apparent}$ vs. [I] replot. *Panel E*, LWB slope vs. [I] replot. *Panel F*,

LWB $1/V_{max,apparent}$ vs. [I]. Km ($\approx$ 180 µM), Vmax ($\approx$ 1130 pmol/min/mg protein), and

Ki (97 µM) values for plots shown were determined using KaleidaGraph (4.1.3). *Panel*

G, chemical structure of 5-4-biphenyl-4-bis-TFM-HMICA.

These data are very difficult to interpret because panels A and B are suggestive of

noncompetitive inhibition while panel C has elements of both competitive and

noncompetitive since the lines are neither intersecting nor parallel. With increasing

inhibitor concentrations there is also an increase in $K_{m, apparent}$ and a decrease in V_{max}

observed for this compound, which is suggestive of mixed inhibition. Therefore, the

mechanism of inhibition for this compound is not fully understood. In addition, since the

Ki value from the 1/Vmax.apparent vs. [I] is considerably higher than that of the slope vs.

[I] plot, this would suggest there is a decreased affinity for which the transporter binds L-

Glu.

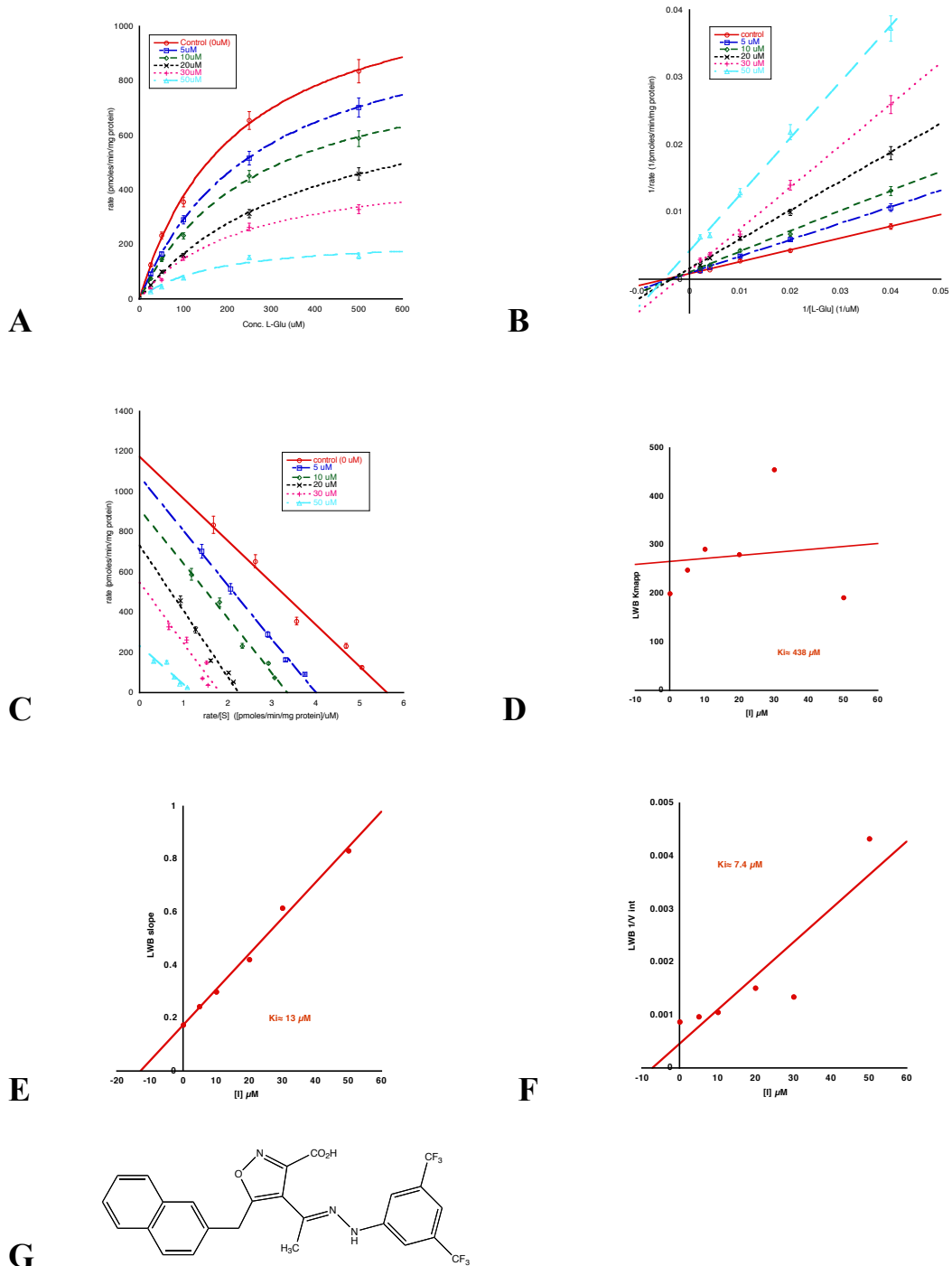**Figure 3.7:** 5-naphthyl-4-bis-TFM-HMICA (**6**) – Noncompetitive Inhibition

Figure 3.7. Legend

Representative kinetic analysis of 5-naphthyl-4-bis-TFM-HMICA **(6)**. *Panel A*,

Michaelis-Menten analysis. *Panel B*, Lineweaver-Burk plot. *Panel C*, Eadie-Hofstee

plot. *Panel D*, LWB $K_{m,apparent}$ vs. [I] replot. *Panel E*, LWB slope vs. [I] replot. *Panel F*,

LWB $1/V_{max,apparent}$ vs. [I]. Km ($\approx$ 220 μM), Vmax ($\approx$ 1200 pmol/min/mg protein), and

Ki (13 μM) values for plots shown were determined using KaleidaGraph (4.1.3). *Panel*

G, chemical structure of 5-naphthyl-4-bis-TFM-HMICA.

This data is consistent with noncompetitive inhibition as seen by the constant $K_{m.apparent}$

values and decreasing Vmax values. This can be seen by lines intersecting at the X-axis

in the LWP plot, and the parallel lines of the Eadie-Hofstee plot. Noncompetitive

inhibition is also demonstrated by the linear $1/V_{max.apparent}$ vs. [I] plot (*panel F*).

Figure 3.8: 5-4-TFM-benzl-4-bis-TFM-HMICA (**7**) – Noncompetitive Inhibition

Figure 3.8. Legend

Representative kinetic analysis of 5-4-TFM-benzl-4-bis-TFM-HMICA **(7)**. *Panel A*,

Michaelis-Menten analysis. *Panel B*, Lineweaver-Burk plot. *Panel C*, Eadie-Hofstee

plot. *Panel D*, LWB $K_{m,apparent}$ vs. [I] replot. *Panel E*, LWB slope vs. [I] replot. *Panel F*,

LWB $1/V_{max,apparent}$ vs. [I]. Km ($\approx$ 190 μM), Vmax ($\approx$ 1200 pmol/min/mg protein), and

Ki (3 μM) values for plots shown were determined using KaleidaGraph (4.1.3). *Panel G,*

chemical structure of 5-4-TFM-benzl-4-bis-TFM-HMICA.

This data is consistent with noncompetitive inhibition as seen by the constant $K_{m.apparent}$

values and decreasing Vmax values. This can be seen by lines intersecting at the X-axis

in the LWP plot, and the parallel lines of the Eadie-Hofstee plot. Noncompetitive

inhibition is also demonstrated by the linear $1/V_{max.apparent}$ vs. [I] plot (*panel F*).

Figure 3.9: 5-4-methoxy-benzyl-4-bis-TFM-HMICA (**8**) - Mixed Inhibition
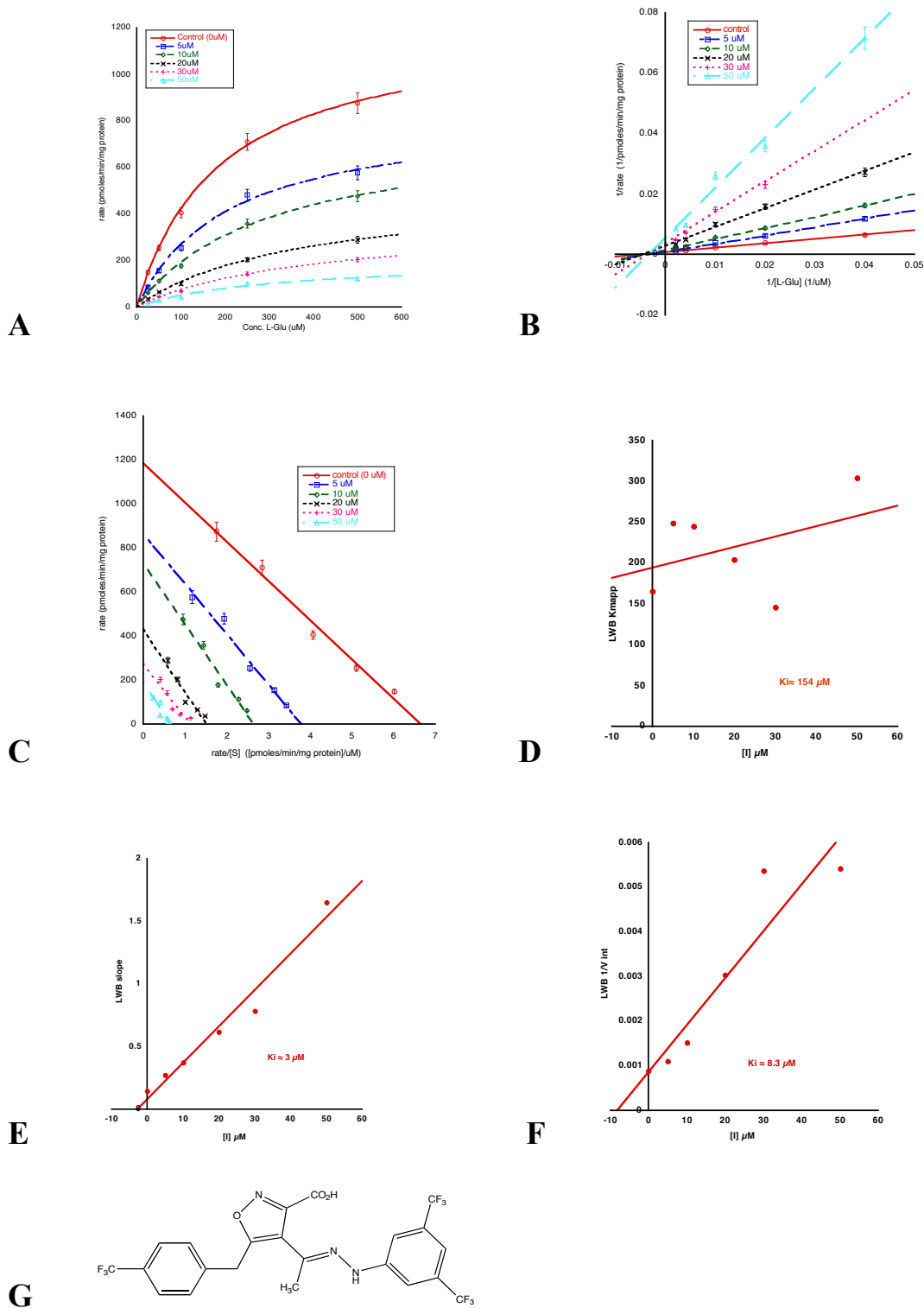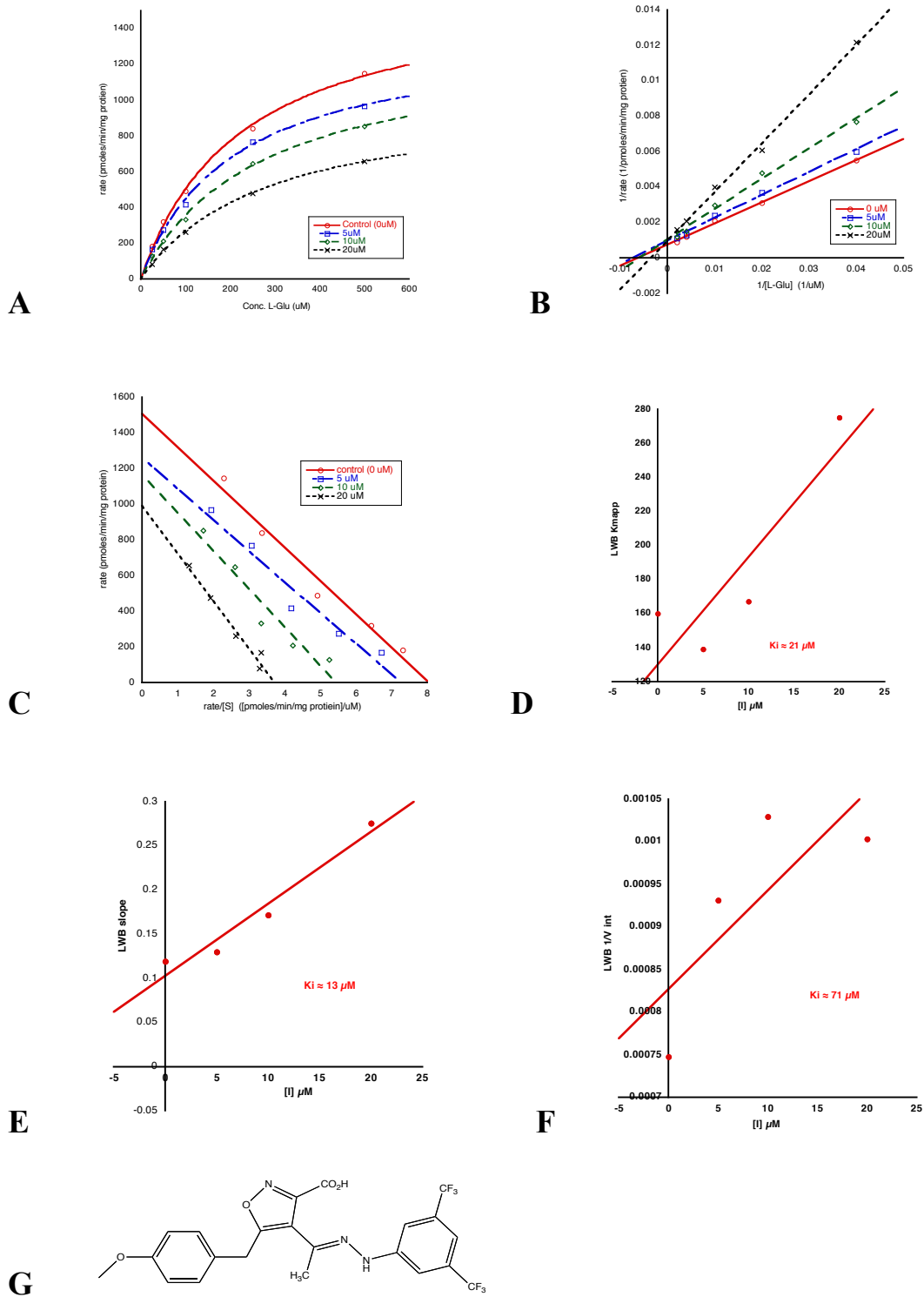

A

B

C

D

E

F

G

Figure 3.8. Legend

Representative kinetic analysis of 5-4-methoxy-benzyl-4-bis-TFM-HMICA **(8)**. *Panel A*, Michaelis-Menten analysis. *Panel B*, Lineweaver-Burk plot. *Panel C*, Eadie-Hofstee plot. *Panel D*, LWB $K_{m,apparent}$ vs. [I] replot. *Panel E*, LWB slope vs. [I] replot. *Panel F*, LWB $1/V_{max,apparent}$ vs. [I]. Km ($\approx$ 230 μM), Vmax ($\approx$ 1650 pmol/min/mg protein), and Ki (13μM) values for plots shown were determined using KaleidaGraph (4.1.3). *Panel G,* chemical structure of 5-4-methoxy-benzyl-4-bis-TFM-HMICA.

These data are very difficult to interpret because panels A and C suggest noncompetitive inhibition while panel B suggests neither noncompetitive nor competitive inhibition. With increasing inhibitor concentrations there is also an increase in $K_{m,\ apparent}$ and a decrease in V_{max} observed for this compound. Therefore, the mechanism of inhibition for this compound is not fully understood. In addition, since the Ki value from the 1/Vmax.apparent vs. [I] is considerably higher than that of the slope vs. [I] plot, this would suggest there is a decreased affinity for which the transporter binds L-Glu.

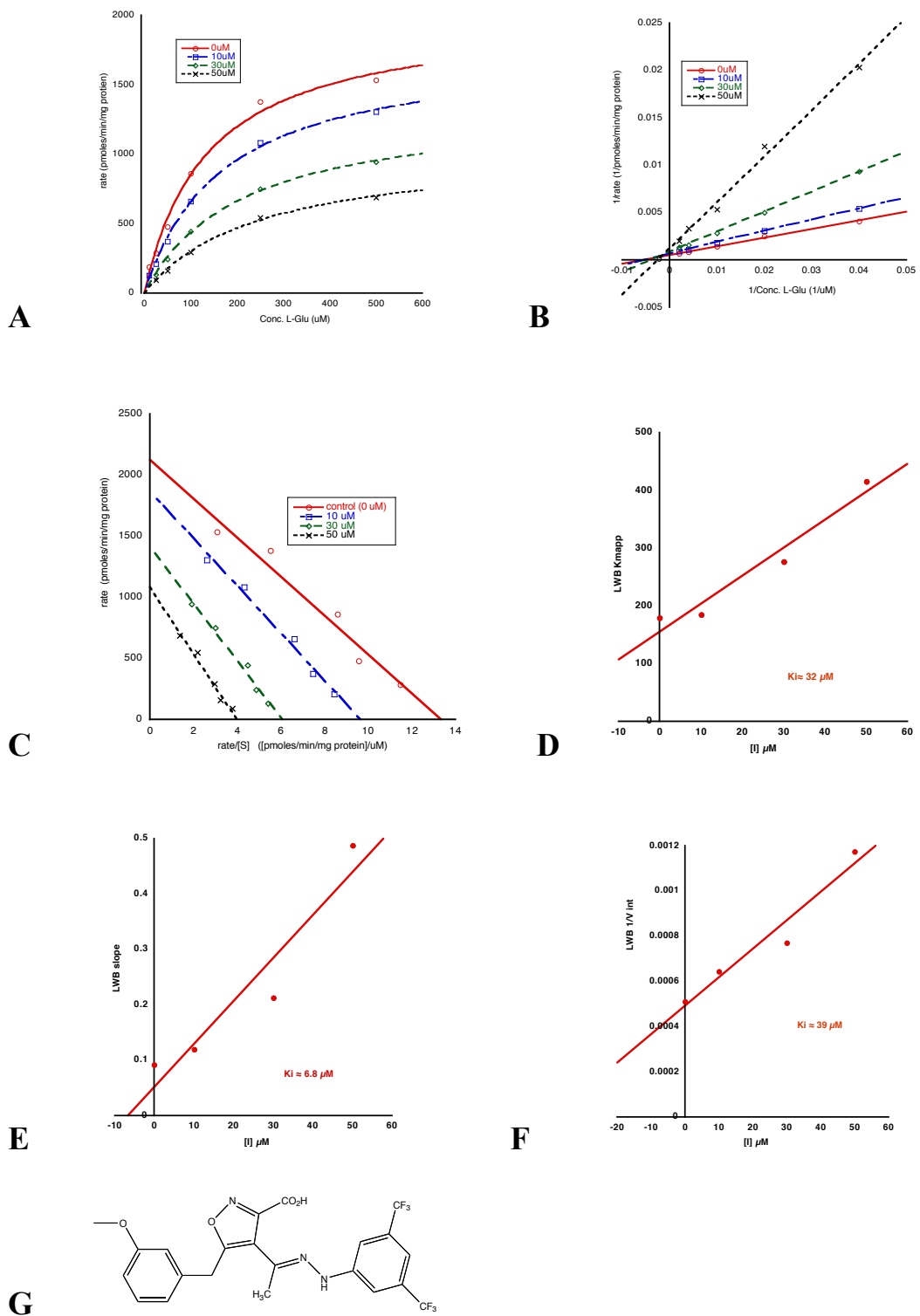**Figure 3.10:** 5-3-methoxy-benzyl-4-bis-TFM-HMICA (**9**)– Mixed Inhibition

Figure 3.10. Legend

Representative kinetic analysis of 5-3-methoxy-benzyl-4-bis-TFM-HMICA **(9)**. *Panel A*,

Michaelis-Menten analysis. *Panel B*, Lineweaver-Burk plot. *Panel C*, Eadie-Hofstee

plot. *Panel D*, LWB $K_{m,apparent}$ vs. [I] replot. *Panel E*, LWB slope vs. [I] replot. *Panel F*,

LWB $1/V_{max,apparent}$ vs. [I]. Km (≈ 140 µM), Vmax (≈ 2000 pmol/min/mg protein), and

Ki (13µM) values for plots shown were determined using KaleidaGraph (4.1.3). *Panel*

G, chemical structure of 5-3-methoxy-benzyl-4-bis-TFM-HMICA.

These data are very difficult to interpret because panels A and C suggest noncompetitive

inhibition while panel B suggests neither noncompetitive nor competitive inhibition.

With increasing inhibitor concentrations there is also an increase in $K_{m,\ apparent}$ and a

decrease in V_{max} observed for this compound. Therefore, the mechanism of inhibition for

this compound is not fully understood. In addition, since the Ki value from the

1/Vmax.apparent vs. [I] is considerably higher than that of the slope vs. [I] plot, this

would suggest there is a decreased affinity for which the transporter binds L-Glu.

Chapter 4. Future directions

The most interesting aspect of my study was the identification of novel inhibitors of Sx_c^- that act through competitive and noncompetitive mechanisms of inhibition. The discovery of noncompetitive inhibitors suggests the possibility for an allosteric binding site on the transporter. Therefore allowing the development of new inhibitors to target a site separate from the substrate binding site. Future development of inhibitors could include a new set of compounds with various alterations to the chemical structure. The development of novel inhibitors containing two lipophilic groups but lacking the L-Glu or L-Cys$_2$ mimic could be used to determine if inhibitory activity remains and to further characterize the lipophilic binding domains. Other possible alterations could be made to the lipophilic domains, the linker group density, or the length of the linker group.

In addition the development of new inhibitors, additional experiments could be done to further characterize the isoxazole hydrazone analogues used in this study. Fluorometric exchange assays could be used to determine substrate activity, to verify the mechanism of inhibition seen using the L-Glu uptake experiments, and to help confirm the presence of a new binding site. Detailed kinetic analysis of early inhibitors (such as 4-S-CPG) could also be done to help delineate the mechanism of inhibition and help to further develop the SAR data at Sx_c^-.

In conclusion, the identification of a new binding site is exciting since it provides the opportunity to develop very potent inhibitors for Sx_c^-. These new inhibitors could lead to clinically relevant outcomes in the brain tumor model.

References:

Augustin H, grosjean Y, Chen K, Sheng Q, Featherstone D (2007). Nonvesicular release of glutamate by glial xCT transporters supresses glutamate receptor clustering in vivo. *J. Neurosci.* **27:** 111-123.

Baker DA, McFarland K, Lake RW, Shen H, Tang XC, Toda S*, et al.* (2003). Neuroadaptations in the cystine-glutamate exchange underlie cocaine relapse. *Nature Neurosci.* **6**(7)**:** 743-749.

Baker DA, Xi ZX, Hui S, Swanson CJ, Kalivas PW (2002). The origin and neuronal function of in vivo nonsynaptic glutamate. *The journal of Neuroscience* **22**(20)**:** 9134-9141.

Bannai S (1986). Exchange of cystine and glutamate across plasma membrane of human fibroblasts. *The Journal of Biological Chemistry* **261**(5)**:** 2256-2263.

Bissantz C, Kuhn B, Stahl M (2010). A medicinal chemist's guide to molecular interactions. *J Med Chem* **53**(14)**:** 5061-5084.

Bridges R, Lutgen V, Lobner D, Baker DA (2012a). Thinking outside the cleft to understand synaptic activity: contribution of the cystine-glutamate antiporter (System xc-) to normal and pathological glutamatergic signaling. *Pharmacol Rev* **64**(3)**:** 780-802.

Bridges R, Natale N, Patel S (2012b). System xc- cystine/glutamate antiporter: an update on molecular pharmacology and roles within the CNS. *British Journal of Pharmacology* **165**(1)**:** 20-34.

Bridges R PS (2009). *Pharmacology of Glutamate Transport in the CNS: Substrates and Inhibitors of Excitatory Amino Acid Transporters (EAATs) and the Glutamate/Cystine Exchanger System xc-*. edn. Springer: NY, NY.

Broer S, Wagner CA (2002). Structure-function relationships of heterodimeric amino acid transporters. *Cell Biochem Biophys* **36**(2-3)**:** 155-168.

Burdo J, Dargusch R, Schubert D (2006). Distribution of the cystine/glutamate antiporter system xc- in the brain, kidney, and duodenum. *J Histochem Cytochem* **54**(5)**:** 549-557.

Dringen R, Pfeiffer B, Hamprecht B (1999). Synthesis of the antioxidant glutathione in neurons: supply by astrocytes of CysGly as precursor for neuronal glutathione. *J Neurosci* **19**(2)**:** 562-569.

Espey MG, Kustova Y, Sei Y, Basile AS (1998). Extracellular glutamate levels are chronically elevated in the brains of LP-BM5-infected mice: a mechanism of retrovirus-induced encephalopathy. *J Neurochem* **71**(5)**:** 2079-2087.

Filomeni G, Rotilio G, Ciriolo MR (2002). Cell signalling and the glutathione redox system. *Biochem Pharmacol* **64**(5-6)**:** 1057-1064.

Gasol E, Jimenez-Vidal M, Chillaron J, Zorzano A, Palacin M (2004). Membrane topology of system xc- light subunit reveals a re-entrant loop with substrate-restricted accessibility. *J Biol Chem* **279**(30)**:** 31228-31236.

Gout PW, Buckley AR, Simms CR, Bruchovsky N (2001). Sulfasalazine, a potent suppressor of lymphoma growth by inhibition of the x(c)- cystine transporter: a new action for an old drug. *Leukemia* **15**(10)**:** 1633-1640.

Halliwell B (2006). Oxidative stress and neurodegeneration: where are we now? *J Neurochem* **97**(6)**:** 1634-1658.

Hosoya K, Tomi M, Ohtsuki S, Takanaga H, Saeki S, Kanai Y*, et al.* (2002). Enhancement of L-Cystine transport activity and its relation to xCT gene induction at the blood-brain barrier by diethyl maleate treatment. *The Journal of Pharmacology and Experimental Therapeutics* **302**(1)**:** 225-231.

Huang Y, Dai Z, Barbacioru C, Sadee W (2005). Cystine-glutamate transporter SLC7A11 in cancer chemosensitivity and chemoresistance. *Cancer Res* **65**(16)**:** 7446-7454.

Janaky R, Ogita K, Pasqualotto BA, Bains JS, Oja SS, Yoneda Y*, et al.* (1999). Glutathione and signal transduction in the mammalian CNS. *J Neurochem* **73**(3)**:** 889-902.

Jimenez-Vidal M, Gasol E, Zorzano A, Nunes V, Palacin M, Chillaron J (2004). Thiol modification of cysteine 327 in the eighth transmembrane domain of the light subunit xCT of the heteromeric cystine/glutamate antiporter suggests close proximity to the substrate binding site/permeation pathway. *J Biol Chem* **279**(12)**:** 11214-11221.

Knackstedt LA, Larowe S, Mardikian P, R. M, Upadhyaya H, Hedden S*, et al.* (2008). The Role of Cystine-Glutamate Exchange in Nicotine Dependence in Rats and Humans. *Biol. Psychiatry* **Epub**.

Leary GP, Holley DC, Stone EF, Lyda BR, Kalachev LV, Kavanaugh MP (2011). The central cavity in trimeric glutamate transporters restricts ligand diffusion. *Proc Natl Acad Sci U S A* **108**(36)**:** 14980-14985.

Lewerenz J, Hewett SJ, Huang Y, Lambros M, Gout PW, Kalivas PW*, et al.* (2013). The cystine/glutamate antiporter system x(c)(-) in health and disease: from molecular mechanisms to novel therapeutic opportunities. *Antioxid Redox Signal* **18**(5)**:** 522-555.

Lyons SA, Chung WJ, Weaver AK, Ogunrinu T, Sontheimer H (2007). Autocrine glutamate signaling promotes glioma cell invasion. *Cancer Res* **67**(19)**:** 9463-9471.

Madayag A, Kau KS, Lobner D, Mantsch JR, Wisniewski S, Baker DA (2010). Drug-induced plasticity contributing to heightened relapse susceptibility: neurochemical changes and augmented reinstatement in high-intake rats. *J Neurosci* **30**(1)**:** 210-217.

Matti AA, Mirzaei J, Rudolph J, Smith SA, Newell JL, Patel SA*, et al.* (2013). Microwave accelerated synthesis of isoxazole hydrazide inhibitors of the system xc-transporter: Initial homology model. *Bioorg Med Chem Lett* **23**(21)**:** 5931-5935.

McDaniel SW, Keyari CM, Rider KC, Natale NR, Diaz P (2011). Suzuki-Miyaura cross-coupling of benzylic bromides under microwave conditions. *Tetrahedron Lett* **52:** 5656-5658.

Muller K, Faeh C, Diederich F (2007). Fluorine in pharmaceuticals: looking beyond intuition. *Science* **317**(5846)**:** 1881-1886.

Nelson JK, Twamley B, Villalobos TJ, Natale NR (2008). The catalytic asymmetric addition of alkyl- and aryl-zinc reagents to an isoxazole aldehyde. *Tetrahedron Lett* **49**(41)**:** 5957-5960.

Newell JL, Keyari CM, McDaniel SW, Diaz PJ, Natale NR, Patel SA*, et al.* (2013). Novel di-aryl-substituted isoxazoles act as noncompetitive inhibitors of the system x cystine/glutamate exchanger. *Neurochem Int*.

Palacin M, Nunes V, Font-Llitjos M, Jimenez-Vidal M, Fort J, Gasol E, *et al.* (2005). The genetics of heteromeric amino acid transporters. *Physiology (Bethesda)* **20:** 112-124.

Patel SA, Rajale T, O'Brien E, Burkhart DJ, Nelson JK, Twamley B, *et al.* (2010). Isoxazole analogues bind the System xc- transporter: Structure-activity relationship and pharmacophore model. *Bioorg Med Chem* **18:** 202-213.

Patel SA, Warren BA, Rhoderick JF, Bridges RJ (2004). Differentiation of substrate and non-substrate inhibitors of transport system x(c)(-): an obligate exchanger of L-glutamate and L-cystine. *Neuropharmacol.* **46:** 273-284.

Reissner KJ, Kalivas PW (2010). Using glutamate homeostasis as a target for treating addictive disorders. *Behav Pharmacol* **21**(5-6)**:** 514-522.

Sagara JI, Miura K, Bannai S (1993). Maintenance of neuronal glutathione by glial cells. *J Neurochem* **61**(5)**:** 1672-1676.

Sasaki H, Sato H, Kuriyama-Matsumura K, Sato K, Maebara K, Wang H, *et al.* (2002). Electrophile response element-mediated induction of the cystine/glutamate exchange transporter gene expression. *J Biol Chem* **277**(47)**:** 44765-44771.

Sato H, Tamba M, Ishii T, Bannai S (1999). Cloning and expression of a plasma membrane cystine/glutamate exchange transporter composed of two distinct proteins. *J Biol Chem* **274**(17)**:** 11455-11458.

Segel I (1993). *Enzyme Kinetics: Behavior and Analysis of Rapid Equilibrium and Steady-State Enzyme Systems*. edn. Wiley.

Seib TM, Patel SA, Bridges RJ (2011). Regulation of the system x(C)- cystine/glutamate exchanger by intracellular glutathione levels in rat astrocyte primary cultures. *Glia* **59**(10)**:** 1387-1401.

Shih A, Erb H, Sun X, Toda S, Kalivas P, Murphy T (2006). Cystine/glutamate exchange modulates glutathione supply for neuroprotection from oxidative stress and cell proliferation. *J. Neurosci.* **41:** 10514-10523.

Singh SK, Piscitelli CL, Yamashita A, Gouaux E (2008). A competitive inhibitor traps LeuT in an open-to-out conformation. *Science* **322**(5908)**:** 1655-1661.

Sontheimer H (2008). A role for glutamate in growth and invasion of primary brain tumors. *J Neurochem* **105**(2)**:** 287-295.

Sontheimer H, Bridges RJ (2012). Sulfasalazine for brain cancer fits. *Expert Opin Investig Drugs* **21**(5)**:** 575-578.

Verrey F, Closs EI, Wagner CA, Palacin M, Endou H, Kanai Y (2004). CATs and HATs: the SLC7 family of amino acid transporters. *Pflugers Arch* **447**(5)**:** 532-542.

Watkins S, Sontheimer H (2012). Unique biology of gliomas: challenges and opportunities. *Trends Neurosci* **35**(9)**:** 546-556.

Ye ZC, Sontheimer H (1999). Glioma cells release excitotoxic concentrations of glutamate. *Cancer Res* **59**(17)**:** 4383-4391.

Zhou P, Zou J, Tian F, Shang Z (2009). Fluorine bonding--how does it work in protein-ligand interactions? *J Chem Inf Model* **49**(10)**:** 2344-2355.

Zurcher M, Diederich F (2008). Structure-based drug design: exploring the proper filling of apolar pockets at enzyme active sites. *J Org Chem* **73**(12)**:** 4345-4361.